PAPER

Fast ion synergistic effects in JET high performance pulses

IOP Publishing | International Atomic Energy Agency Nuclear Fusion

Nucl. Fusion **59** (2019) 056005 (19pp) https://doi.org/10.1088/1741-4326/ab02ae

Fast ion synergistic effects in JET high performance pulses

K.K. Kirov[1], Yu. Baranov[1], I.S. Carvalho[2], C.D. Challis[1], J. Eriksson[3], D. Frigione[4], L. Garzotti[1], J. Graves[5], P. Jacquet[1], D.L. Keeling[1], E. Lerche[6], P.J. Lomas[1], C. Lowry[7], M. Mantsinen[8,9], F. Rimini[1] and JET Contributors[a]

EUROfusion Consortium, JET, Culham Science Centre, Abingdon OX14 3DB, United Kingdom of Great Britain and Northern Ireland

[1] CCFE Fusion Association, Culham Science Centre, Abingdon, United Kingdom of Great Britain and Northern Ireland

[2] Instituto de Plasmas e Fusão Nuclear, Instituto Superior Técnico, Universidade de Lisboa, 1049-001 Lisboa, Portugal

[3] Department of Physics and Astronomy, Uppsala University, SE-75120 Uppsala, Sweden

[4] Unità Tecnica Fusione—ENEA C. R. Frascati—via E. Fermi 45, 00044 Frascati (Roma), Italy

[5] Ecole Polytechnique Fédérale de Lausanne (EPFL), Swiss Plasma Center (SPC), CH-1015 Lausanne, Switzerland

[6] Lab. for Plasma Phys. KMS-ERM Renaissancelaan, 30 Avenue de la Renaissance B-1000, Brussels, Belgium

[7] European Commission, B-1049 Brussels, Belgium

[8] Barcelona Supercomputing Center, Barcelona, Spain

[9] ICREA, Pg. Lluís Companys 23, 08010 Barcelona, Spain

E-mail: Krassimir.Kirov@ukaea.uk

Received 30 October 2018, revised 21 December 2018
Accepted for publication 29 January 2019
Published 22 March 2019

Abstract

Fast ion synergistic effects were studied by predictive modelling of JET best performing pulses for various levels of neutral beam injection (NBI) and radio frequency (RF) power. Calculated DD neutron yields were analysed with the intention of separating the impact of RF synergistic effects due to changes in fast ion (FI) distribution function (DF) from secondary effects accompanying the application of RF power, namely changes in T_e and T_i. A novel approach in analysing the efficiency of fast ions in fusion reactions based on evaluation of the cumulative reaction rates is outlined and used in the study. Conclusions on the impact of fast ion synergistic effects on fusion performance are based on comparisons of beam-target (BT) and thermal (Th) DD reaction rates. It was found that changes in auxiliary heating power, NBI and RF, by 4 MW will affect DD fusion performance and neutron rates significantly. Simulations of the best performing JET pulses show that for H minority RF heating scheme with available RF power the impact of RF synergistic effects is somewhat lesser than the secondary effects related to changes in T_e and T_i. In conditions of much higher RF power the modification in fast ion distribution function (FI DF) and the impact of the fast ions on BT DD fusion becomes significant. The impact of the RF and NBI power on the BT reactivities was found to be of similar order; however, the NBI power has greater impact on reaction rates due to its larger effect on fast ion density.

Keywords: NBI/ICRH synergy, fast ion distribution function, predictive modelling, JET

(Some figures may appear in colour only in the online journal)

[a] See the author list of Litaudon *et al* [61].

1. Introduction

One of the key requirements for achieving high fusion performance in today's tokamaks is injecting high neutral beam injection (NBI) power. The beam particles injected with initial energy in the region of 80–120 keV create high-energy fast ion populations in the hot plasma core. Adding radio frequency (RF) power leads to interaction between wave electric field and NBI ions, providing the wave particle resonance condition is satisfied, and this process further modifies the fast ion distribution function (FI DF). This phenomenon is commonly referred to as 'synergistic effects' and it has been a subject of intensive studies as reported in [1–9] and more recently in [10–13]. Better understanding of the physics involved in fast ion (FI) synergistic effects is important for dealing with two essential issues in present fusion research: (i) improving the beam-target (BT) fusion performance measured by the BT neutron rate in stable plasma conditions and (ii) mitigating the negative effect of the interactions between highly energetic particles and various MHD modes.

The need for comprehensive investigation of the interactions between NBI fast ions and RF waves in JET has been addressed in a series of recent publications [10–13]. They focus on better understanding the synergistic effects in view of achieving high BT fusion performance. Simulations with JETTO/PION codes of JET's best performing hybrid pulses have been carried out [13] and important conclusions have been made regarding RF minority schemes, resonance position and minority concentrations. Deuterium–Tritium (DT) mixture plasmas have been studied extensively in early JET [14–20] and TFTR [20–23] DT campaigns and it has been highlighted that synergetic effects have a key role in achieving high BT fusion performance.

Fast ion synergistic effects will certainly have implications for JET with the forthcoming DT campaign [24] and future ITER operations [25, 26]. A considerable effort in modelling and optimisation of JET DT neutron yield was carried out in parallel to the recent JET experimental campaign [27]. The main focus of this task was on predictive transport modelling in view of extrapolating from present Deuterium plasma conditions to a DT mixture. In addition to the transport studies it has been recognised [27] that synergistic effects of the NBI fast ions will have a considerable contribution to the expected BT DT fusion performance. Indeed, the maximum of the DT cross-section in the centre-of-mass energy frame is about 64 keV, which number translates for D beams energy into cold T target of about 107 keV and for T beam energy into cold D target of about 160 keV. JET's NBI full energy component is of the order of 80–120 keV for D beams, i.e. near the maximum of DT cross-section. The full energy component for T beams is similar, but due to the different form of the cross-section curve for T beam into DT plasma this is below energy required for maximum reactivity. This suggests that fine tuning of the FI DFs for resonant DT reactions can help maximise the fusion yield. Synergistic effects play an important role in this optimisation of the BT fusion performance and the studies reported here address this issue and contribute towards a better understanding of the physics involved.

Neutron rate is a commonly used measure of the fusion performance of neutron producing nuclear reactions. Principal contributions are BT and thermal rates. The former is due to collisions of beam fast ions with thermal plasma, while the thermal rates only account for nuclear reactions between bulk thermal ions. Regarding BT neutrons, in this study we focus on two main issues related to fast ion synergistic effects. First, to assess the contribution of RF synergistic effects resulting from the application of RF power in NBI heated plasma. The term 'RF synergistic effect' is used here to refer to the effects due to modification of the FI DF whereas the term 'secondary effects' refers to changes in electron and ion temperatures, T_e and T_i, from NBI and RF heating. Both T_e and T_i depend strongly on the applied RF and NBI power and separating them from contributions due to RF accelerated fast ion in the analysis of the BT fusion performance requires closer look at the deuterium fast ions distribution function. RF power for instance, changes the electron temperature, T_e, which will affect the fast ion slowing down and hence will affect the BT neutron rate. Changes to ion temperature, T_i, on the other hand will strongly affect the thermal nuclear reactions and to some extent BT reactions. For this reason, BT and thermal rates are studied separately in this paper.

An additional objective of this study is to investigate how different power levels from NBI and RF affect the fusion performance. Detailed examination of the FI DF and DD reaction rates in D plasmas heated with D NBI and RF tuned to fundamental H minority and harmonic D frequency, has been carried out to asses which of the two auxiliary heating systems at JET, NBI or RF, has a greater impact on the fusion performance. The aim here is to investigate the operational conditions and plasma parameters at which BT DD neutron yield or equally the BT DD fusion reaction rates can be maximised. Maximising the input NBI and RF power is an obvious choice, but they impact differently on FI DF as it is shown in this paper. NBI power tend to act directly on the FI DF in the beam energy region, 40–120 keV also called plateau in FI DF here, while RF power in addition to this can pull a high energy tail in the distribution function. The plateau and the tail of FI DF have a different impact on the BT DD fusion performance and studying this is one of the main subjects of this paper.

Whilst an increase in BT reaction rates is not directly relevant to future fusion reactors which require high thermal yield, methods to increase BT reaction rate are of interest in experiments which, for example, require large energetic alpha populations or even high neutron fluxes to test plasma facing components properties. A robust methodology to separate RF synergistic and secondary effects is also useful in allowing any improvement in thermal reaction rate to be accurately determined.

Experiments from the high power JET campaign in 2016 are discussed and analysed here. Two complementary operational scenarios were developed at JET as main candidates for sustained high DT fusion power [28]: the baseline scenario with normalised beta, $\beta_N \sim 1.8$, and the hybrid scenario with $\beta_N \sim 2$–3. The baseline scenario development [29] concentrates mainly on pushing the operation towards the high current and field limits with a relaxed current profile, whereas

the hybrid experiments focus mainly on the advantages of operating at high β_N with a shaped current profile and central safety factor above 1. Best performing pulses from both scenarios were used in the study. Fully predictive modelling was carried out and reported in [29]. In addition, here power scans were used to investigate the dependence of the reaction rates on the input power. Analysing the data by means of predictive modelling, as was done here, allows for scans in the parametric space as well as separation of various contributions to the investigated neutron rates. An alternative method would be to analyse the database of JET pulses. In these studies, however, this is not helpful in finding underlying parametric dependencies. One of the disadvantages of this approach is that the number of the pulses required for a basic scan in parametric space increases significantly with the number of parameters and values to be scanned. In addition, the fact that many of the input parameters are highly correlated complicates the analysis considerably. For instance, RF power will change electron and ion temperature hence by using database analysis method there will be no clear indication of whether T_i and T_e changes or synergistic effects due to application of RF power have the greatest impact on the neutron rates. As an example to illustrate this, figure 1 shows the neutron yield versus diamagnetic energy, which is a measure of the plasma pressure, in all high-power baseline pulses at JET in 2016 campaign. The total neutron yield increases almost exponentially with plasma energy as measured by the magnetic measurements. This trend is an indicator of high fusion performance achieved in these pulses. Color-coded points depict the dependencies on the applied RF power in (*a*) and central electron temperature in (*b*). Clearly pulses with high diamagnetic energy need higher RF power in order to achieve higher neutron rate; however, similar dependence is seen with regard to electron temperature as well. Obviously, this kind of analysis is incapable of distinguishing between the impact of the RF synergistic and secondary effects on the fusion performance. Thus, in this paper the preferred method of analysis is by predictive modelling of the fusion performance by scanning the input RF and NBI power.

Simulations of the best performing JET pulses show that for H minority/harmonic D heating scheme with available RF power the impact of RF synergistic effects is somewhat lesser than the secondary effects with varying heating power. In conditions of much higher RF power the modification in FI DF and the impact of the fast ions on DD fusion becomes significant. The impact of the RF and NBI power on the BT reactivities was found to be of similar order; however, the NBI power has greater impact on reaction rates due to its larger effect on fast ion density. This paper is organised as follows: section 2 gives details on the numerical codes used. In section 3 important diagnostics on which this study heavily relies are discussed together with the high-performing baseline and hybrid pulses. Detailed physical picture of the FI DF modifications by NBI energy and RF electric field are provided in section 4. Results are presented in section 5 where the findings of the predictive modelling and the power scans are highlighted. Section 6 is dedicated to conclusions and discussions.

2. Modelling tools used in the study

A substantial part of the study is based on predictive transport modelling and analysis of fast ions distribution functions. Routine predictive transport modelling at JET is usually performed with the JETTO code [30] coupled to PION/PENCIL package for computing NBI and RF power absorptions taking into account the synergistic effects. Preference to JETTO over other available transport modelling codes was given because it allows for use of Bohm-gyroBohm model. This is a distinctive semi-empirical model which gives reasonable agreement with a large proportion of JET experimental data [31], using a combination of Bohm and gyro-Bohm terms in the heat diffusivity expression.

The PION code [32] is used in JETTO for ICRH minority and harmonic heating utilising its main advantage of being computationally fast thus compatible with integrated modelling. The code interfaces with the existing PENCIL NBI deposition code [33, 34] and accounts for NBI and RF synergy effects [35] thus providing flux-surface averaged FI DF and RF power deposition self-consistently with plasma density and temperature.

In addition to the predictive JETTO modelling the TRANSP [36–39] code was used in interpretive runs to provide FI DFs and BT reactivities as well. The NUBEAM code [40] is a computationally comprehensive Monte Carlo code for NBI injection in tokamaks. The code follows the fast ion trajectories and takes into account orbit effects in fast ion distribution calculations which is its main advantage over PENCIL.

Although PION/PENCIL code can in general provide an estimate of FI DFs, in reality TRANSP/NUBEAM was given preference for this task for several reasons. First, the orbit effects are treated in a simplified way in PION; however, due to its simplicity, they are neglected in PENCIL thus important physics of the fast ion distribution and confinement is missing in this treatment. NUBEAM is a MC code and it follows the fast ions orbits and accounts for all orbit effects. In addition, the nature of the analysis reported here requires a correct estimate of the local FI DFs which are poloidally inhomogeneous; however, PION/PENCIL can only deal with flux surface averaged FI DF. In fact, PION/PENCIL provides the total (thermal + FI) distribution functions which makes it inappropriate in our case as the purpose of the analysis is to separate the role of the synergistic effects in BT reactivities. FI DF could be extracted from the total distribution function by subtracting the thermal Maxwellian part but this process was deemed to introduce additional uncertainties in the analysis.

The principal RF wave solver for TRANSP is the TORIC code [41]. In TRANSP, TORIC is coupled to a Fokker–Planck solver, FPP [42], which adds bounce averaging treatment. To study the ion cyclotron (IC) resonance of the heated ions, FPP code was used to calculate the RF power absorption by H minorities and the collisional transfer to the bulk D ions and electrons. Monte Carlo quasi liner RF kick operator [43, 44] was implemented in NUBEAM and used to calculate the absorption of RF power by energetic fast D ions. The RF wave solver in TRANSP, TORIC, provides information about RF electric field components and perpendicular wave

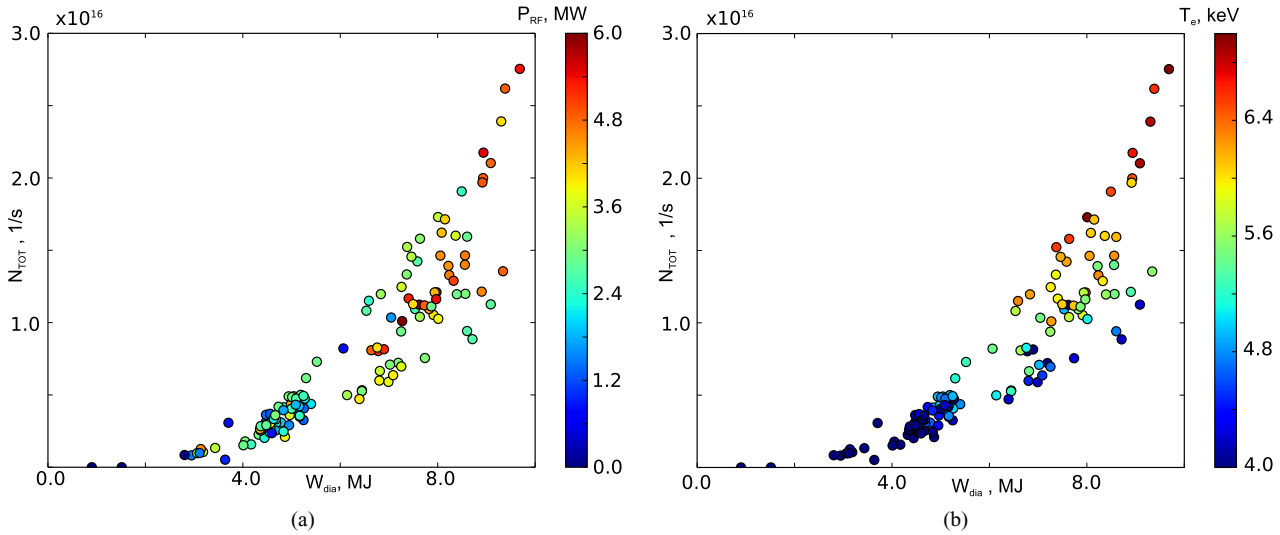

Figure 1. Neutron yield, N_{TOT}, versus diamagnetic plasma energy, W_{dia}, for baseline database with colour-coded RF power P_{RF} in (*a*) and electron temperature T_{e} in (*b*).

vector for each toroidal mode. RF resonance condition for a given harmonic is then used to calculate the magnetic moment and energy of the particles satisfying the resonant condition. Assuming that the resonant ions lose their phase information with RF wave by collisions and wave stochasticity before they re-enter the resonance layer a random walk model can be used to reproduce the stochastic nature of RF heating in magnetic moment space. Every time fast ion passes through resonance layer it receives a kick in magnetic moment space. The magnitude of the kick is derived from the quasi-linear theory, while the stochastic nature is reproduced by means of Monte Carlo random number for the phase of the gyro-orbit [43, 44]. Details of the implementation of RF kick operator in NUBEAM code and results of various benchmarking tests are provided in [45]. At present there is no feedback from NUBEAM's FI DF to TORIC.

3. Experimental setup

3.1. Essential diagnostics

Experimental data from standard JET diagnostics and recommended signals were used in the study. Density profiles and electron temperature profiles were taken from the High Resolution Thomson Scattering diagnostics, HRTS, and/or light detection and ranging, LIDAR, measurements [46]. Electron temperature from ECE radiometer [47] was also included in the analysis. Radiated power was measured by the bolometric diagnostics. Neutron production rates were taken from the available neutron yield monitors.

The effective charge, Z_{eff}, and the main impurity species in plasma have an important influence on the calculated neutron rates. In our studies Z_{eff} was assessed by means of Bremsstrahlung measurements from visible spectroscopy. Uncertainties in determination of main impurity have been studied at JET [48] and it has been shown that calculated neutron rates vary by about 20% depending on whether low (Be) or mid-Z impurity (Ni) is used. Recent studies on mid-Z impurities in JET plasma using a VUV diagnostic [49] indicated that the principal impurity in high power discharges is Ni.

After the change of JET wall from C to Be and W metallic ITER like wall (ILW) traditional charge-exchange spectroscopy for T_{i} measurements, heavily relying on CVI spectra analysis, has become considerably more difficult. A combination of diagnostics was used to deduce T_{i} for the investigated pulses: x-ray crystal spectroscopy (XCS), charge exchange recombination spectroscopy (CXRS) and neutron spectrometer. Uncertainties in T_{i} measurements will affect the neutron rates. The thermonuclear rates in the analysed temperature range are roughly proportional to $T_{\mathrm{i}}^{2.5}$ so errors in their assessment are approximately 2.5 times larger than those of T_{i} measurements. BT reaction rates also depend on T_{i}, as shown later on figure 5 a), and for the purposes of the analysis here it has been assessed that a 30% variation of T_{i} will result in 15% changes in BT neutron rates.

3.2. JET neutron spectrometer TOFOR

Data from JET neutron time-of-flight spectrometer (TOFOR) were exclusively used in the neutron spectra analysis. The TOFOR diagnostic is described in detail in [50, 51]. It has a vertical line of sight through the plasma core and perpendicular to the magnetic field covering the region between 2.74 m $< R_{\mathrm{maj}} <$ 3.02 m. TOFOR consists of two sets of plastic scintillator detectors. First is placed in the collimated flux of neutrons from the plasma and the second is placed 1.2 m away at an angle of 30° to the beam direction. A fraction of the incoming neutrons scatter in the first detector and then some of them are detected by the second one. The time of each scattering event is recorded and from the two arrays of scattering times a time-of-flight (TOF) spectrum is constructed. The energy of incoming neutrons is determined by the TOF related to the measured distance between the two detectors. DD neutrons, which typically have energies of about 2.5 MeV, give rise to flight times around 65 ns. The full response function of

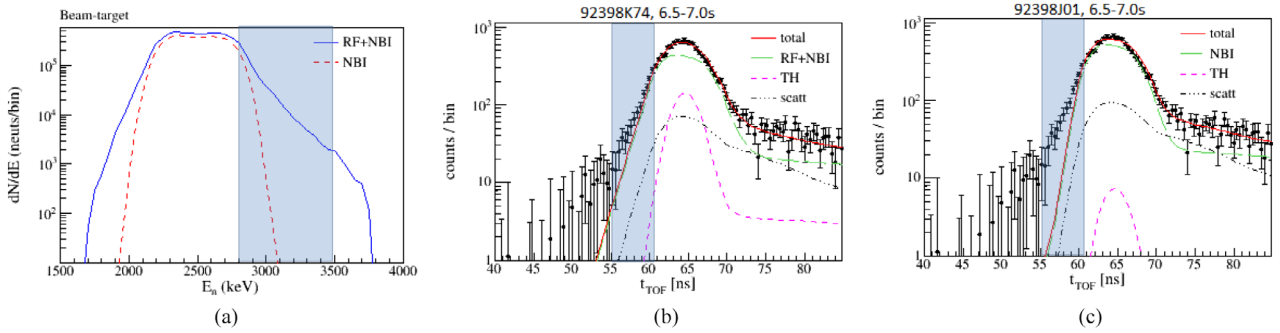

Figure 2. (*a*) Beam-target DD 2.45 MeV neutron production spectra computed as described in [52] showing that RF contributions can be clearly identified for neutron energies $E_n < 2$ MeV and $E_n > 2.8$ MeV; (*b*) TOFOR analysis compared to simulated t_{TOF} for hybrid pulse #92398 with $P_{NB} = 27$ MW and $P_{RF} = 5$ MW showing good agreement between simulations and measurements; (*c*) TOFOR analysis compared to simulated t_{TOF} for hybrid pulse #92398 with $P_{NB} = 27$ MW and assuming zero RF power and lower T_e and T_i showing that the high energy (short time-of-flight, <61 ns) part of the spectrum does not match the TOFOR data for 55 ns $< t_{TOF} <$ 61 ns.

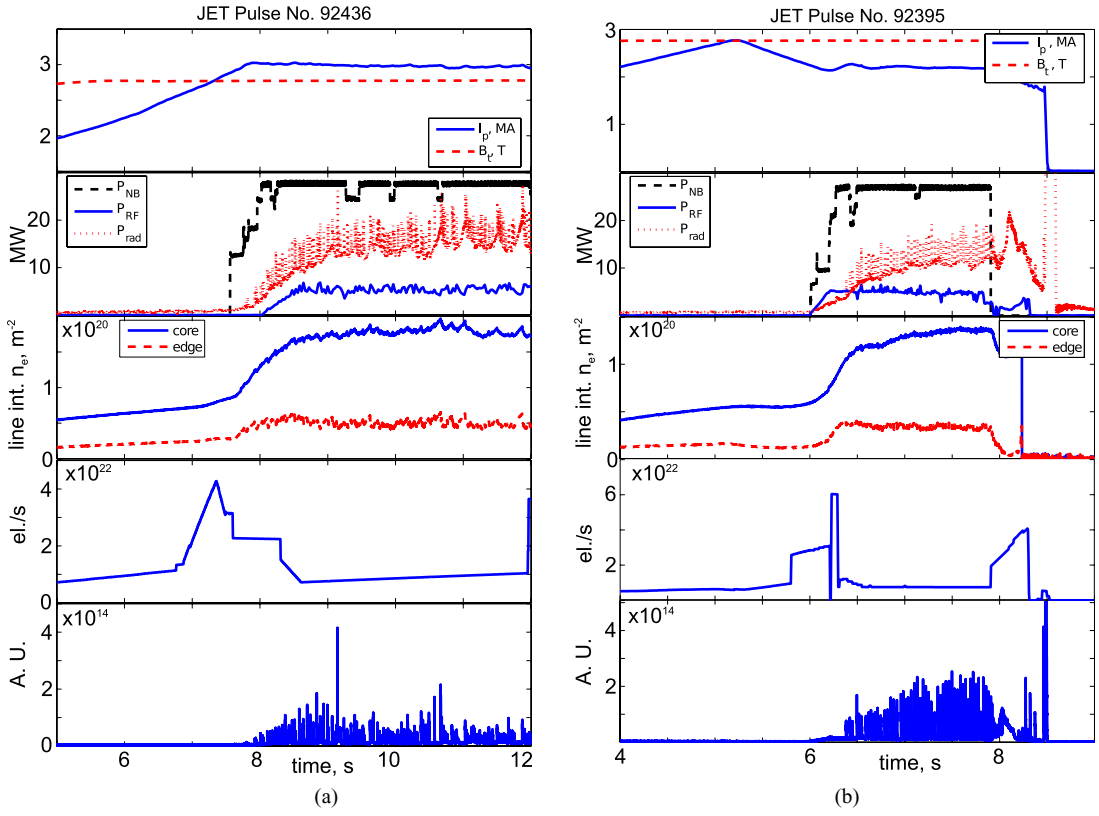

Figure 3. (*a*) Time traces of JET pulse #92436, 2.8 T/3 MA high performance baseline, top to bottom, I_p/B_t, $P_{NB}/P_{RF}/P_{rad}$, core and edge line integrated density, total gas dosing rate and ELMs from BeII spectroscopy; (*b*) same as (*a*) but for JET pulse #92395, 2.8 T/2.2 MA high performance hybrid.

TOFOR has been calculated with Monte Carlo methods [52]. For the cases simulated and discussed here TOFOR time-resolution is a limiting factor; in order to obtain data with reasonable confidence one has to integrate over 0.5 s around the time of interest.

Beam-target neutron spectra, dN/dE, for NBI+RF and NBI only cases are shown in an illustrative example in figure 2(*a*). Significant enhancement of dN/dE by the RF power is expected for lower, $E_n < 2$ MeV, and higher energies, $E_n > 2.8$ MeV. Monoenergetic beams with energies of 100 keV and 500 keV are expected to create double-humped shaped neutron spectra with high-energy peaks at $E_n = 2.8$ MeV and $E_n = 3.5$ MeV respectively. These estimates of E_n correspond to $t_{TOF} = 61$ ns and $t_{TOF} = 55$ ns [51]. This constitutes the basis of detection of fast ions created by RF by means of the TOFOR diagnostic and neutron energy ranges and t_{TOF} time which correspond to these values are highlighted in figure 2. TOFOR data are compared to simulated data with $P_{NB} = 27$ MW and $P_{RF} = 5$ MW figure 2(*b*). In addition, a case where RF power was assumed to be zero and 10% lower T_e and T_i is shown in figure 2(*c*). The good match of t_{TOF} in the range 55 ns to 61 ns in figure 2(*b*), which is the band where RF effects are most clearly observed (given in grey in figure 2) suggests the FI DF from TRANSP run with

5 MW of RF power matches reasonably well the experimental observations. On the other hand, the calculation assuming no RF power, hence no FI DF tail, figure 2(*c*), clearly contradicts TOFOR observation for t_{TOF} between 55 ns and 61 ns.

3.3. JET high performance baseline and hybrid pulses

The baseline [28] development experiment on JET [29] featured a number of high performing pulses at high plasma current and input power. Pulse #92436, figure 3(*a*), had characteristics: 3 MA/2.8 T (top graph) with line integrated density of $\approx 1.8 \times 10^{20}$ m^{-2} (line averaged of about 6.4×10^{19} m^{-3}) and central $T_{e0} \approx 7.3$ keV and T_i near the plasma core of about 8–9 keV. NBI power of about $P_{NB} = 27.5$ MW (figure 3(*a*) second graph from the top) was applied right at the end of the current ramp up at 7.55 s. ICRH power in dipole at 42.5 MHz was ramped from 8.05 s and reached its maximum of about $P_{RF} = 5.2$ MW half a second later for H minority heating, while the radiated power measured by the bolometric measurements was about 40% of the total input power. Gas dosing (figure 3(*a*) fourth graph from the top) during the main heating phase increases from $\approx 6.4 \times 10^{21}$ el s^{-1} to about 9.4×10^{21} el s^{-1} with H concentration of about 3% of the total electron density. Small 2 mm pellets were fired with frequency of about 45 Hz from 8.5 s to 13 s to maintain plasma density and sustain regular ELMs (figure 3(*a*) bottom graph). Pellets are fired only into the periphery of the plasma, so that their impact could be modelled by gas dosing only. Type I ELMs with frequency of about 30 Hz were observed up until ≈10.6 s. The pulse featured reasonable confinement enhancement with H98 ≈ 1.1, relatively high normalised beta, $\beta_N \approx 2$, and neutron rate up to 2.8×10^{16} s^{-1}. The pulse was modelled in TRANSP and by JETTO from the start of the main heating phase, 7.5 s, up until 9.4 s.

JET pulse #92935, figure 3(*b*), was one of the best performing hybrid scenario [28] pulses in the last JET campaign regarding neutron rates. The pulse was carried out as part of hybrid scenario development experiment and its main parameters are as follows: 2.2 MA/2.75 T (figure 3(*b*) top graph), line integrated density $\approx 1.3 \times 10^{20}$ m^{-2} (figure 3(*b*) third graph from the top, line averaged of about 4.6×10^{19} m^{-3}), central $T_{e0} \approx 7.8$ keV and T_i near the core of about 8 keV were achieved by means of $P_{NB} = 27$ MW of NBI power and $P_{RF} = 5$ MW of ICRH (figure 3(*b*) second graph from the top) in dipole at 42.5 MHz for H minority heating with steady radiation assessed by bolometric measurements to be of about 30% of the total input power. Gas dosing during the main heating phase was about 7×10^{21} el s^{-1} maintaining steady ELMs with frequency of about 35 Hz while the target H minority concentration was kept of about 1.5%. Confinement was of the order of H98 ≈ 1.3 for about 1 s from the start of the main heating. Normalised beta $\beta_N \approx 2.5$ was sustained throughout the pulse, while neutron rates up to 2.7×10^{16} s^{-1} were measured, which is one of the highest for ILW hybrid pulses. Large fishbones and $n = 3$ mode were observed at about 7.9 s. A main chamber hot spot alarm at 7.9 s triggered controlled termination of the pulse a few hundred milliseconds after that (at about 8.4 s). The pulse was modelled in TRANSP and by JETTO from the start of the main heating phase, 6 s, up until 7.8 s.

4. Impact of RF electric field on NBI fast ions

Results presented in this study will be discussed by means of fusion reactivities and reaction rates. For the cross-section, σ, reactivity, $\sigma \cdot v$, and the averaged reactivity, $\langle \sigma \cdot v \rangle$, standard notations, definitions and units are used. Averaged reactivity by the thermal (Th) ions is noted as $\langle \sigma \cdot v \rangle_{Th}$, while for BT reactions $\langle \sigma \cdot v \rangle_{BT}$ notation is used. In addition, BT reactivities are assessed by means of formula (7) from Mikkelsen paper [53]. This formula, which here will be referred to as $\langle \sigma \cdot v \rangle_{BT\_MEB}$, is a good approximation for BT reactivities in D(d, n)^{3}He reactions and beam energies of up to 0.7 MeV. It takes into account the temperature of the target plasma but is only valid for monoenergetic beams (MEB). The expression for the full BT reactivity $\langle \sigma \cdot v \rangle_{BT}$ can be derived in principle after integration of the product of $\langle \sigma \cdot v \rangle_{BT\_MEB}$ f_{fi} over fast ion energies, where $f_{fi}(E)$ is normalised FI DF, $\int_0^\infty f_{fi}(E')\mathrm{d}E' = 1$. The latter is related to the total FI DF, $F_{fi}(E) = n_{fi} f_{fi}(E)$, via the fast ion density, n_{fi}. In order to assess the contribution of the fast ions to the BT fusion performance, the product $\langle \sigma \cdot v \rangle_{BT\_MEB} F_{fi}$ as a function of fast ion energy, E, and the cumulative integral of it will be used in the study. The latter is calculated in the interval [0, E] and is also presented as a function of E. For infinitely large E the cumulative integral is equal to $n_{fi} \langle \sigma \cdot v \rangle_{BT}$, which is also used for consistency checks. By using the product $\langle \sigma \cdot v \rangle_{BT\_MEB} F_{fi}$ and the cumulative integral of it as a function of the energy instead of the full integral, an estimate of how fast ions contribute to BT reactivity can be made. In this way the contribution of high energy fast ions to the BT fusion performance can be highlighted. For instance, as the synergistic effects will impact on FI DF the change of the value of the cumulative integral due to changes in RF power will show directly the impact of the RF synergistic effects. Reaction rate is proportional to the densities of the reactants and averaged reactivity, i.e. $R_{BT} = n_{fi} n_D \langle \sigma \cdot v \rangle_{BT}$ and $R_{Th} = n_D^2 \langle \sigma \cdot v \rangle_{Th}/2$, where n_{fi} and n_D are the fast ion and bulk deuterium densities. Volume integral of R_{BT} and R_{Th} will provide the total number of neutrons per second, $N_{TOT} = N_{BT} + N_{Th}$, from the plasma. This can be measured with good accuracy over a wide range of energies by the available neutron detectors at JET. The beam–beam (BB) neutron rates are assessed to be at least two orders of magnitude lower than thermal and BT rates, so this contribution is neglected in the analysis.

In NBI heated only plasma BT rate will depend strongly on the beam energy, E_b, the plasma electron density, n_e, and temperatures, T_e and T_i, as well as the effective charge of the plasma, Z_{eff}. The JET NBI system usually operates with beam acceleration voltage in the range 40–120 keV. FI DF decreases sharply with energy for $E > E_b$, usually few orders of magnitude in few tens of keV. If RF power is applied in addition to NB injection of D, the neutron production will be affected in various ways. Indeed, adding RF power to NBI fuelled/heated D plasma can have an

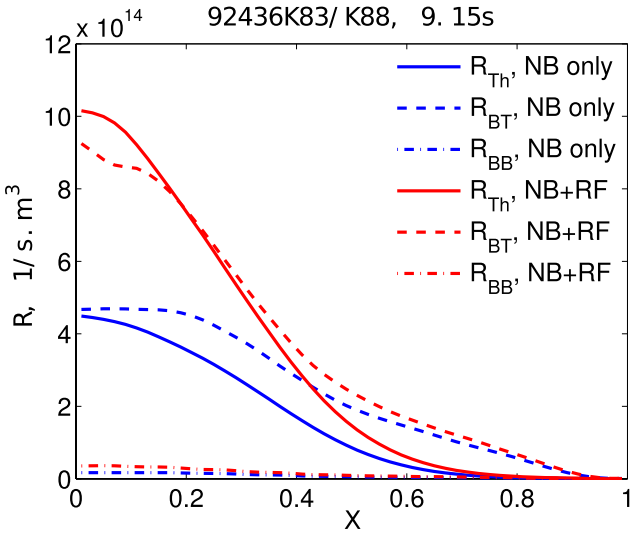

Figure 4. Flux surface averaged thermal, subscripts Th, BT and BB, reaction rates versus TRANSP normalised toroidal flux radius, X, for JET best performing baseline pulse #92436 with NBI power only in blue and NBI+RF in red.

impact on a number of plasma parameters: for instance ion and electron temperatures, T_i and T_e. In turn, electron temperature changes can affect beam deposition, slowing down and fast ion distributions hence BT reactions, while T_i has an indirect (via fast ion slowing down) and direct (via changes in $\langle\sigma \cdot v\rangle_{Th}$ and $\langle\sigma \cdot v\rangle_{BT}$) impact on thermal and BT rates. RF will also require a minority specie which could affect D bulk ions' density and thus cause fuel dilution. In the investigated (H)D minority scheme, the H minority will be heated at $n = 1$ fundamental cyclotron frequency, while the bulk D ions will be heated via collisions with minorities and at $n = 2$ harmonic cyclotronic frequency by the RF field. The FI DF of D beam ions will be also affected by the RF power directly as fast D beam ions can also absorb energy directly from the RF wave at $n = 2$ harmonic cyclotron frequency providing wave-particle resonance condition is satisfied. RF wave with frequency near $n = 2$ harmonic ion cyclotron D resonance modifies the FI DF as a high energetic tail is created in the plasma core for energies a few times larger than the injected beam energy, E_b. The plateau region of FI DF, for energies $E \geqslant E_b/3 \approx 40$ keV and $E \leqslant E_b \approx 120$ keV, is modified as well.

The thermal, BT and BB reaction rates profiles for two cases, with and without RF power in a typical JET pulse calculated by TRANSP [36–39] are shown in figure 4. In both cases, NBI only and NBI+RF, thermal and BT rates are peaked in the very core and small for normalised toroidal flux radius $X > 0.4$–0.5. For example, in the case discussed in figure 4 the BT rates inside $X < 0.5$ provide about 67% of the total BT neutrons, whilst the thermal rates inside this volume are even higher, about 84% of the total thermal neutrons. BB rates are insignificant, usually two orders of magnitude smaller than BT rates, and therefore they will be ignored in the study. Figure 4 shows that RF power affects both thermal and BT rates making them larger (red curves) and even more peaked in the centre of the plasma.

In the core, $X < 0.2$, the resonant RF wave creates a high energy tail with energies $E > 120$ keV in the FI DF and this will affect BT reactivity $\langle\sigma \cdot v\rangle_{BT}$. An example of monoenergetic beam BT reactivity $\langle\sigma \cdot v\rangle_{BT\_MEB}$ versus beam energy E, FI DF $F_{fi}(E) = n_{fi} f_{fi}(E)$ representative of a 2D cell in the plasma centre, their product, $\langle\sigma \cdot v\rangle_{BT\_MEB} F_{fi}(E)$, and BT cumulative reaction rate $R_{BT}(E)$ for NBI only (blue lines) and NBI+RF (red lines) heating is shown in figure 5. As expected BT reactivity $\langle\sigma \cdot v\rangle_{BT\_MEB}$ increases with beam energy, however, this increase is relatively small for energies $E > 300$ keV compared to the range $E = 50$–300 keV, figure 5(a). The fully evolved FI DF $F_{fi}(E) = n_{fi} f_{fi}(E)$ provided by TRANSP for time interval larger than a few slowing down times, and the Maxwellian distribution function, F_{Th}, in figure 5(b) both calculated at the same point, show the energy at which the bulk provides more particles than NBI to interact with RF wave. Clearly for T_i in the range 6–8.4 keV and for fast ion energies $E > 50$ keV there are more D beam ions to interact with RF wave than D ions from the bulk Maxwellian distribution, figure 5(b). This might seem to contradict to the widely accepted approximation that RF absorption by given particles depends on particle pressure, $n\,T$. However, this relies on the assumption that the distribution function is Maxwellian, which is not valid for FI DF studied here. High energetic tail associated with RF is clearly present for energies greater than $E > E_b \approx 120$ keV, red line in figure 5(b). The origin of this tail is clearly due to fast D beam ions. One should also note that RF power modifies the plateau of $F_{fi}(E)$, with energies in the range $E > E_b/3 \approx 40$ keV to $E < E_b \approx 120$ keV and these changes are essential in BT reaction rate enhancement as it can be seen from $\langle\sigma \cdot v\rangle_{BT\_MEB} F_{fi}$ versus E graph in figures 5(c) and (d). The BT reaction rate $R_{BT}(E)$ in figure 5(d) is presented as a function of E, where E is the upper limit of the cumulative integral, i.e. $R_{BT}(E) = n_D\, n_{fi} \langle\sigma \cdot v\rangle_{BT}(E) = n_D \int_0^E \langle\sigma \cdot v\rangle_{BT\_MEB} F_{fi}(E')\, dE'$. Hereafter, we will refer to $R_{BT}(E)$ as BT cumulative reaction rate to distinguish from the conventional definition of BT reaction rate $R_{BT} = R_{BT}(E \to \infty)$. Fast ions with energies up to about 120 keV are the main contributor in R_{BT}: in NBI only case (blue lines in figures 5(c) and (d)) 98% of BT neutrons originate from BT reactions with fast ions with energies $E < E_b \approx 120$ keV, while in the NBI+RF example (red lines in figures 5(c) and (d)) approximately 2/3 of R_{BT} is due to fast ions with $E < E_b \approx 120$ keV. In the latter case the FI DF tail contributes 1/3 to DD BT rates.

Figure 5(b) shows that in the plasma core the RF power will clearly impact on FI DF tail and plateau. Which of these will be affected more depends on the plasma and RF parameters and RF heating scenario. Detailed assessment requires self-consistent modelling including NBI and RF heating and particle and heat transport. Modification to FI DF plateau and tail will have a different impact on BT and thermal neutrons and hence on the BT fusion performance.

For comparison, the impact of the electron and ion temperatures, T_e and T_i, in the NBI only case in figure 5 has been studied. Reduction of any of T_e or T_i by about 30% from the reference will result in reaction rate drop of 15%. Decrease in T_e for instance will affect the plateau region and to a smaller

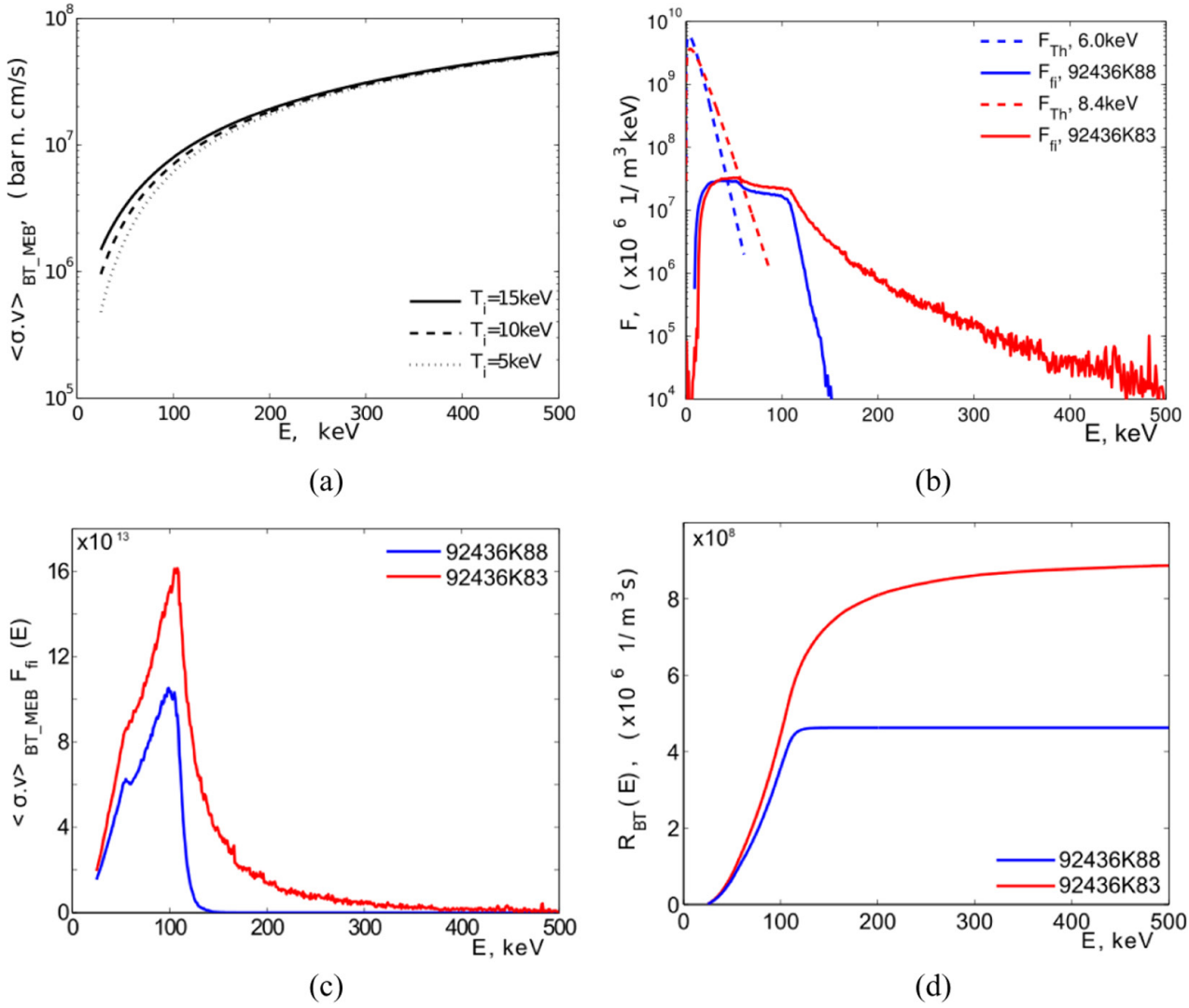

Figure 5. (*a*), BT reactivity from Mikkelsen [46] formula (7), $\langle\sigma \cdot v\rangle_{\mathrm{BT\_MEB}}$, for mono-energetic beam as a function of fast D ion energy for three values of target D ion temperature; (*b*), bulk Maxwellian (F_{Th}, dashed lines) and fast ion (F_{fi}, solid lines) unnormalized distribution functions near magnetic axis for baseline pulse #92436, 9.18 s near magnetic axis ($R = 3$ m, $Z = 0.23$ m) as provided by TRANSP with (red lines) and without (blue lines) RF power; (*c*), the product $\langle\sigma \cdot v\rangle_{\mathrm{BT\_MEB}}\, F_{\mathrm{fi}}$ as function of fast ion energy for the two cases shown above; (*d*), BT cumulative reaction rate $R_{\mathrm{BT}}(E)$ as explained in the text.

extent the tail of FI DF in the plasma core. The plateau in FI DF will go up with T_{e}, which will lead to an increase in BT neutron rates. Lower T_{i} is expected to impact on the FI DF plateau and tail hence BT rates in addition to the thermal rates. The changes in the FI DF tail by varying T_{e} and T_{i} are always negligible in comparison with RF generated tail in FI DF, red line in figure 5(*b*). This way, by using the product $\langle\sigma \cdot v\rangle_{\mathrm{BT\_MEB}}\, F_{\mathrm{fi}}$ as a function of fast ion energy, E, and the cumulative reaction rates as the ones shown in figures 5(*c*) and (*d*) one can easily assess the contribution by the RF generated tail in FI DF from secondary effects of T_{e} and T_{i} on FI DF. For this purpose, graphs as in figures 5(*c*) and (*d*) will be extensively used for the analysis presented in the next sections.

5. Results

Results of the predictive modelling are discussed first in detail in the next section. They provide a basis for power scan studies presented subsequently. Fully predictive modelling of the reference base line and hybrid pulses was performed initially to validate the transport model used here versus the available experimental data. This model is then used in the power scans studies, which provide the FI DF evolution with NBI and RF heating power.

5.1. Predictive modelling of stationary phases

In JETTO, electron density, n_{e}, electron and ion temperatures, T_{e} and T_{i}, were modelled predictively by means of the Bohm-gyroBohm model [31]. Although the progress in modelling with first principle models is significant [27, 54] the preferred model in this study is the Bohm-gyroBohm model because it provides simplicity and it has been observed to produce good results in previous studies. Predictive modelling of the reference pulses was performed initially in order to validate the transport model versus available experimental data and

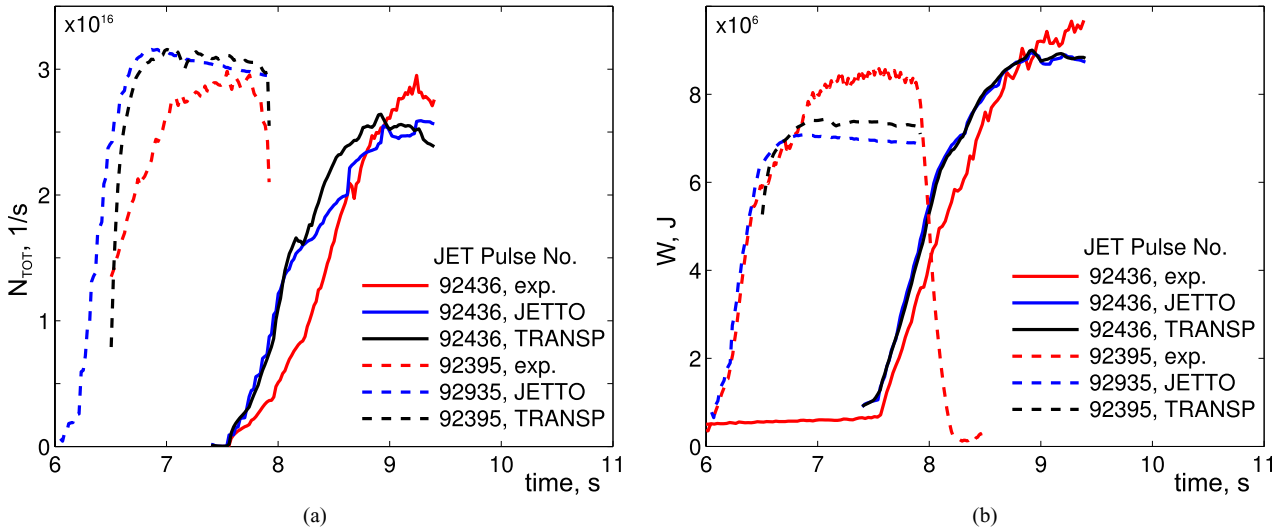

Figure 6. (*a*) Total neutron yields, N_{TOT}, and (*b*) stored plasma energy, W_{p}, measured (in red) and from JETTO predictive (in blue) and TRANSP (in black) runs for baseline pulse #92436 (solid lines) and hybrid pulse # 92395 (dashed lines).

to confirm it can be used to extrapolate to higher/lower input heating power. In power scans studies, as the ones reported here, keeping transport model settings fixed is essential and it was regarded that the Bohm-gyroBohm model is best suited for this purpose. H-mode physics is treated with JETTO's own edge barrier transport model, while ELMs were emulated with ELM criteria model. The FRANTIC code was used to treat neutrals. Effective charge Z_{eff} is assumed radially constant with time variations as provided by the available spectroscopic diagnostics. For baseline pulse #92436 the effective charge Z_{eff} increases in time from about 1.5 to 2.1 with averaged values of about 1.85, while for the hybrid pulse #92395 it varies between 1.6 and 2.2 with averaged value of 1.81. The main impurity specie in the simulations is assumed to be Ni ($Z = 28$, $A = 59$) in agreement with recent JET observations [49]. The radiated power is taken from the available bolometric measurements. In this way, electron and ion sources were calculated self-consistently with the NBI and RF heating and equilibrium kinetic plasma profiles.

FI DFs and reaction rates are further extracted from a follow-up TRANSP interpretive run. For this purpose, TRANSP was run interpretively with kinetic profiles as produced in the corresponding JETTO simulation. The local FI DFs and BT reactivities are thus available from TRANSP/NUBEAM for analysis and calculation of cumulative reaction rates.

Time traces of calculated and measured total neutrons stored plasma energy, W_{p}, and total neutron rate, N_{TOT}, are provided in figure 6. Both these quantities are extremely sensitive to T_{i} and fast ion density and energies. For that reason, achieving a good agreement between modelled and experimental data as shown in figure 6 provides important validation that the transport models are applicable to these cases.

The two codes, JETTO and TRANSP, agree reasonably well in calculated total neutrons, N_{TOT}; averaged values differ by less than 1% for #92436 (averaged in 8.5–9.4 s) and #92395 (averaged in 7–7.5 s). As for the plasma energy, W_{p}, we have a discrepancy of about 1% between the two codes for #92436 and about 5% for #92395, figure 6(*b*). The consistency between JETTO and TRANSP results should come as no surprise as in both cases identical kinetic profiles were used.

The agreement between the simulated (JETTO and TRANSP) and the experimental data for the neutron yield is 8% for the baseline pulse #92436. Measured neutrons, N_{TOT}, are 10% lower compared to TRANSP result for #92395 and 8% lower than the JETTO prediction, figure 6(*a*). Agreement with W_{p} data is reasonable, about 5% between measured and calculated for #92436. For the hybrid pulse #92395 the measured W_{p} is 11% higher compared to TRANSP result and 15% larger compared to for JETTO, figure 6(*b*).

The simulation results for electron density and temperature and ion temperature profiles of baseline pulse #92436 are shown in figures 7(*a*)–(*c*), respectively. Experimental profiles are provided for comparison as well.

Electron temperature, T_{e}, was slightly overestimated at the mid-radius in the simulations, while T_{i} was in good agreement with pedestal CX data for $X > 0.7$. Various additional T_{i} measurements were used to constrain the analysis in the plasma core. Standard core CXRS measurements on JET were not of satisfactory quality, so data from the NeX CXRS line (shown in figure 7(*c*)) were used instead. Additional estimates of the central T_{i} was available through crystal spectrometer (XCS) and TOFOR diagnostics, figure 7(*c*), and the simulations are in reasonable agreement with these estimates. It is worth noting that the core T_{i} is strongly coupled to the edge transport barrier parameters. Higher core T_{i} as suggested by the measurements, however, leads to a poor agreement: the calculated neutron rates and plasma energy will be much higher than the measured ones. In general, achieving perfect match between modelled and all available experimental data, n_{e}, T_{e}, T_{i} profiles and N_{TOT} and W_{p} time traces is practically impossible so results presented in figure 7 are considered a reasonable compromise regarding the available experimental data.

Similar results were obtained for the high performance hybrid pulse #92395, figure 8. Here again, the simulated

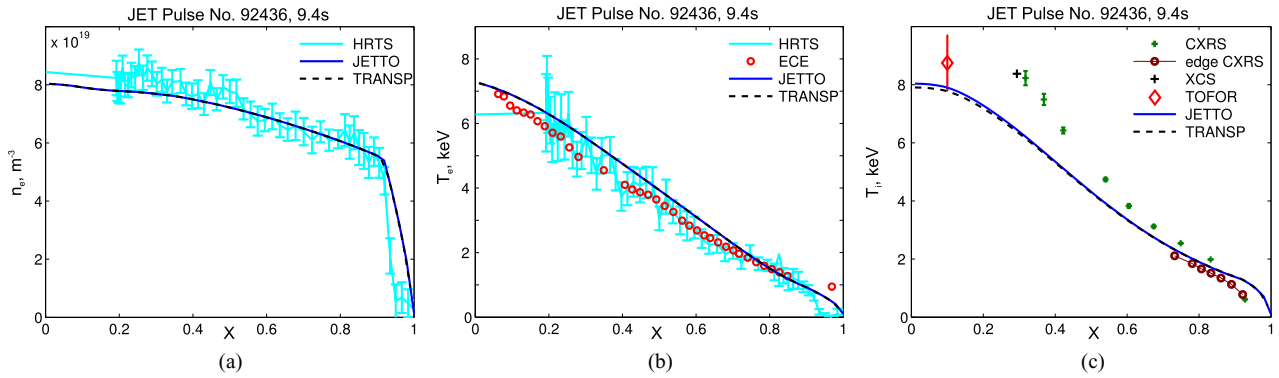

Figure 7. Baseline pulse #92436, n_e, T_e, T_i profiles at 9.4 s from JETTO predictive modelling with BgB model compared to the experimental profiles from the available diagnostics. TRANSP (black dashed lines) was run with profiles provided by JETTO (blue solid lines), hence the profiles are overlapped.

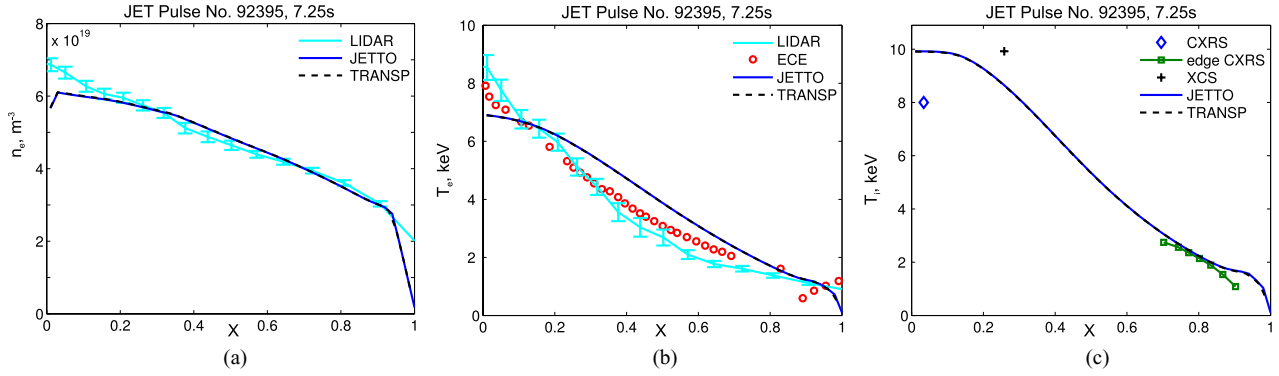

Figure 8. Hybrid pulse #92395, n_e, T_e and T_i profiles at 7.25 s from JETTO and TRANSP interpretive analysis compared to the experimental profiles from the available diagnostics. TRANSP (black dashed lines) was run with profiles provided by JETTO (blue solid lines), hence the profiles are overlapped.

electron temperature, T_e, was overestimated at the mid-radius, for $0.2 < X < 0.7$. The modelled central electron temperature is 13% lower than the ECE measurements, while for $X = 0.5$ it is about 20% higher. Predictive simulations with a first principles physics model [55] were tried and successfully reproduced T_e evolution; however, this was achieved at the expense of quality of n_e and T_i profiles. It was deemed that the small inconsistency in T_e by Bohm-gyroBohm model, figure 8(*b*), will only contribute marginally to the neutron rates. Assessment of the impact of T_e on neutron rates for NBI heated plasma is provided at the end of section 4. It is worth noting that despite the small differences in measured and calculated T_e profiles the Bohm-gyroBohm model produces reasonably well the neutron rates in the investigated time interval, figure 6(*a*). Ion temperature data for the hybrid pulse, #92395, are shown in figure 8(*c*). The standard CXRS diagnostic provided only a single point near the core, $X \approx 0.05$, which is in a reasonable agreement with data from BeII lines (not shown in the graph). Predicted T_i by JETTO is higher and in reasonable agreement with crystal spectrometer data (XCS). The agreement with pedestal CX diagnostic is also reasonable.

The profiles from JETTO predictive models were then used in TRANSP simulations to assess fast ion contributions to neutron yields. The combined use of two codes, JETTO and TRANSP, intended to provide detailed insight into fast ion physics. JETTO with coupled PION/PENCIL provides self-consistent density and temperature profiles and NBI and RF power depositions. TRANSP with NUBEAM coupled to TORIC code was run interpretively with fixed profiles as from JETTO and 64 000 Monte Carlo markers. The advantage of this approach is two-fold. First, it allows us to deduce the local FI DFs, which in turn were used to analyse reactivity' and reaction rate dependencies on fast ion energies. Secondly, the NUBEAM code contains more detail than PENCIL as it treats more accurately the fast ion confinement and orbit effects.

The output of FI DFs from TRANSP is further validated versus neutron spectra analysis by a synthetic TOFOR diagnostic. The analysis of the DD neutron times-of-flight is discussed below.

TRANSP data for the FI DF from pulse #92436 were used in TOFOR analysis and results of simulated and measured time-of-flight are shown in figure 9(*a*), while data from pulse #92395 are shown in figure 9(*b*). Overall, the agreement is reasonable. The match to the experimental data for baseline #92436 is good for the whole region of interest with 55 ns $< t_{TOF} <$ 61 ns, figure 9(*a*), validating the FI DF produced by TRANSP. For the hybrid pulse, #92395, again good agreement was observed for time-of-flight between 57 ns and 61 ns. The region with flight times smaller than 57 ns, however, is systematically underestimated by TRANSP, indicating that TOFOR detects more RF accelerated deuterons than

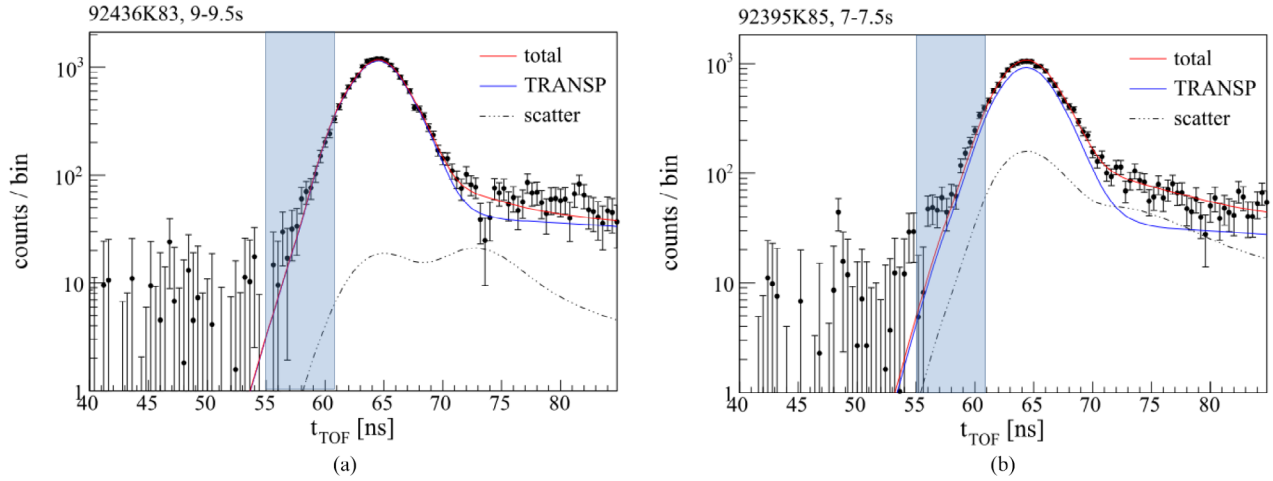

Figure 9. (*a*) TOFOR analysis for JET pulse #92436, averaged in 9–9.5 s, simulated total TOFOR spectra (red line) from TRANSP with $P_{RF} = 5$ MW (blue line) and scattered neutrons contribution (black dash-dotted line) compared to time-of-flight measurements (black dots); (*b*) same as (*a*) but for TRANSP run for hybrid pulse #92395.

TRANSP predicts. This implies that the synergistic effects by the RF kick operator in TRANSP are conservative and effects could be even larger than what is shown in the subsequent modelling.

5.2. Power scans

Two types of power scans are discussed here. First one is by varying the input NBI and RF power by a small amount (4 MW) compared to the total input power (33 MW) and analysing the response of BT and thermal neutron rates and the FI DF. The second scan is performed by switching off the RF power in cases with and without changes to the kinetic plasma profiles. The aim of the latter is to distinguish contributions from the RF synergistic effects from the secondary effects accompanying the application of RF power.

Changes to the FI DFs and resulting cumulative neutron rates by varying the NBI and RF power are accounted for by modifying the auxiliary heating by about 4 MW, i.e. 12% of the total input power. This is a good compromise between achievable heating power capabilities at JET and the requirement for a small variation of the input power to probe the synergistic effects. For the reference cases of JET pulses #92436 and #92395 varying the heating by 4 MW means changing NBI power by 15% and RF power by 70%–80%. The latter implies RF power of about 9–9.5 MW which is somewhat above the present capabilities of the JET ICRH plant. The focus of the analysis is, however, not to extrapolate fusion performance with auxiliary power rather than to study the impact of the NBI and RF power on the FI DF and this is only possible if the NBI and RF power are varied in equal amounts. The applied NBI power was varied between 23 MW and 32 MW by changing the NBI energy while keeping all the available beam lines. The advantage of this approach is that the geometrical parameters of the beam lines are kept unchanged during simulations. NBI and RF powers have different impacts on the FI DF, figure 5, as the former is expected to impact mainly in the plateau region 40–120 keV, while RF power is expected to pull an energetic tail for $E > 120$ keV. Performing the power scan by varying P_{NB} and P_{RF} will also show in what energy range changes to the FI DF are more beneficial regarding fusion performance.

Two additional cases without RF power are considered as well; one with plasma parameters corresponding to $P_{RF} = 0$ predictive run, the other without RF heating but with kinetic profiles as from the reference case for which $P_{RF} \neq 0$. The aim of this comparison is to separate impact of the RF synergistic effects from secondary effects resulting from the application of RF power as for instance the impact of T_e and T_i changes with P_{RF}.

Reasonably good modelling data matching well the experimental measurements and kinetic profiles as seen in figures 6–8 confirm the utilisation of Bohm-gyroBohm model in the predictive studies. Changing the heating power however may have indirect impact on several parameters which could affect the particle and heat transport. For instance, it is known [56] that large P_{RF} can mitigate the impurity accumulation and hence the radiated power. On the other hand, if the RF power is not sufficiently high the source of heavy impurities due to sheath effects will dominate over the impurity screening effect of the RF heating [56]. This contribution was not accounted for in the power scan reported here. Another example is H-mode pedestal pressure scaling with input power. In our study we use an empirical expression based on a global confinement and pedestal database [57]. Recent studies [58] of JET ILW database has found that the scaling of the pedestal stored energy with heating power is only slightly lower than that used in [57]. Providing a small change in the heating power is used, about 12%, and due to the fact that power dependence is weak the two studies [57, 58] agree reasonably well, within about 1%, on the predicted pedestal energy. Therefore, using formula (2) from Cordey *et al* [57] and assuming unchanged top of the barrier (TOB) density provides a suitable scaling expression for the electron and ion temperature at TOB. The latter is calculated to be of the order of 0.9–1 keV for the refence cases, while varying NBI or RF

Table 1. Results of power scan simulations of JET baseline pulse #92436 at 9.15 s. NBI and RF power are provided in columns 2 and 3 followed by FI, main D ion and electron densities and temperatures, BT and thermal averaged reactivities and reaction rates. All these quantities are volume averaged, noted by $\langle\rangle$, inside plasma volume $0 < X < 0.4$. The last three columns provide the time averaged, 8.9–9.4 s, BT, thermal and total number of reactions. The first row in the table gives the absolute values of these quantities for the reference case with actual NBI and RF power. Rows #1 to #6 show the relative changes of the quantities with respect to the reference case. Bottom two rows, #5 and #6, are both for $P_{RF} = 0$ but row #5 is with plasma parameters corresponding to $P_{RF} = 0$ while #6 is with plasma parameters as in the reference case. Changes larger than 7% are in bold.

#92436	P_{NB}, MW	P_{RF}, MW	$\langle n_{fi}\rangle$, m^{-3}	$\langle n_D\rangle$, m^{-3}	$\langle n_e\rangle$, m^{-3}	$\langle T_e\rangle$, keV	$\langle T_i\rangle$, keV	$\langle\langle\sigma v\rangle_{BT}\rangle$, $m^3\ s^{-1}$	$\langle\langle\sigma v\rangle_{Th}\rangle$, $m^3\ s^{-1}$	$\langle R_{BT}\rangle$, $1/m^3\ s$	$\langle R_{Th}\rangle$, $1/m^3\ s$	N_{BT}, 1/s	N_{Th}, 1/s	N_{TOT}, 1/s
reference	27.5	5.7	2.53×10^{18}	7.05×10^{19}	7.51×10^{19}	5.799	6.647	3.26×10^{-24}	2.13×10^{-25}	5.70×10^{14}	4.92×10^{14}	1.48×10^{16}	9.77×10^{15}	2.52×10^{16}
#1	23.4	5.7	**0.75**	1.00	0.99	**0.90**	**0.86**	**0.81**	**0.67**	**0.61**	**0.67**	**0.64**	**0.66**	**0.64**
#2	31.6	5.7	**1.37**	1.02	1.02	**1.07**	**1.11**	**1.25**	**1.31**	**1.74**	**1.34**	**1.70**	**1.35**	**1.57**
#3	27.5	1.7	**0.89**	1.02	1.02	**0.83**	**0.84**	**0.80**	**0.62**	**0.72**	**0.64**	**0.79**	**0.64**	**0.73**
#4	27.5	9.7	**1.13**	0.98	0.98	**1.15**	**1.09**	**1.25**	**1.24**	**1.39**	**1.18**	**1.26**	**1.20**	**1.24**
#5	27.5	0	**0.84**	1.03	1.03	**0.75**	**0.73**	**0.73**	**0.39**	**0.62**	**0.42**	**0.69**	**0.43**	**0.59**
#6	27.5	0	0.96	1	1	1	1	**0.89**	1	**0.85**	1	**0.91**	1	0.95

Table 2. Same as table 1 but for power scan simulations of JET hybrid pulse #92395 for time slice at 7.25 s. The last three columns provide the time averaged, 7.0–7.5 s, BT, thermal and total reactions. Bottom two rows, #5 and #6, are both for $P_{RF} = 0$ but row #5 is with plasma parameters corresponding to $P_{RF} = 0$ while #6 is with plasma parameters as in the reference case. Changes larger than 7% are in bold.

#92395	P_{NB}, MW	P_{RF}, MW	$\langle n_{fi}\rangle$, m^{-3}	$\langle n_D\rangle$, m^{-3}	$\langle n_e\rangle$, m^{-3}	$\langle T_e\rangle$, keV	$\langle T_i\rangle$, keV	$\langle\langle\sigma v\rangle_{BT}\rangle$, $m^3\ s^{-1}$	$\langle\langle\sigma v\rangle_{Th}\rangle$, m^3/s	$\langle R_{BT}\rangle$, $1/m^3s$	$\langle R_{Th}\rangle$, $1/m^3s$	N_{BT}, 1/s	N_{Th}, 1/s	N_{TOT}, 1/s
reference	26.8	5.2	5.24×10^{18}	5.07×10^{19}	5.64×10^{19}	5.691	8.343	3.63×10^{-24}	4.07×10^{-25}	9.73×10^{14}	4.88×10^{14}	1.98×10^{16}	9.34×10^{15}	3.10×10^{16}
#1	22.8	5.2	**0.80**	1.00	0.98	**0.93**	**0.89**	**0.83**	**0.75**	**0.66**	**0.76**	**0.67**	**0.75**	**0.69**
#2	30.8	5.2	**1.35**	0.95	0.99	**1.10**	**1.14**	**1.26**	**1.38**	**1.60**	**1.24**	**1.60**	**1.25**	**1.53**
#3	26.8	1.1	**0.87**	1.06	1.05	**0.84**	**0.84**	**0.77**	**0.63**	**0.71**	**0.72**	**0.75**	**0.72**	**0.73**
#4	26.8	9.3	**1.12**	0.95	0.96	**1.14**	**1.09**	**1.27**	**1.25**	**1.36**	**1.12**	**1.30**	**1.14**	**1.27**
#5	26.8	0	**0.84**	**1.07**	1.06	**0.80**	**0.77**	**0.72**	**0.50**	**0.64**	**0.59**	**0.68**	**0.59**	**0.65**
#6	26.8	0	0.94	1	1	1	1	**0.87**	1	**0.81**	1	**0.86**	1	**0.90**

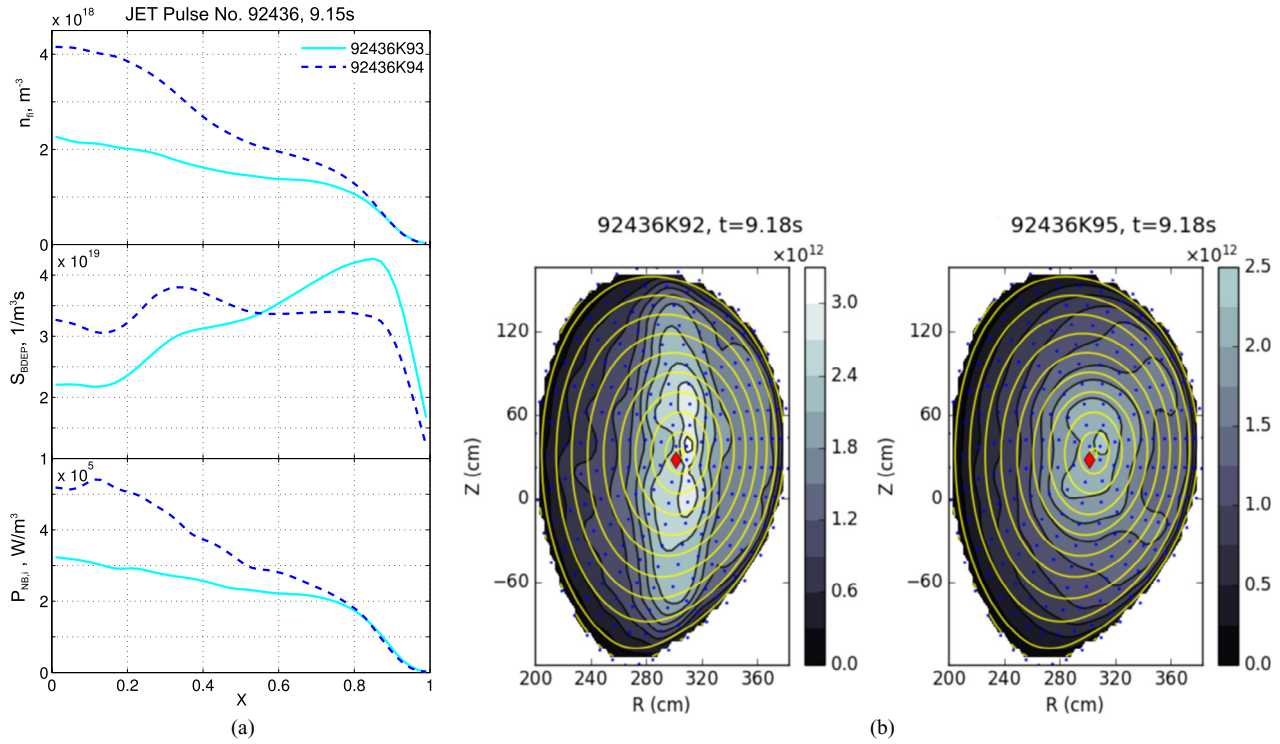

Figure 10. (*a*) Baseline pulse #92436, simulations for $P_{\rm NB} = 23.4$ MW, case #1 in table 1 (cyan solid lines), and $P_{\rm NB} = 31.6$ MW, case #2 in table 1 (blue dashed lines), comparison of fast ion densities $n_{\rm fi}$ (top), beam deposition $S_{\rm BDEP}$ (middle) and NBI ion heating $P_{\rm NB,i}$ (bottom) profiles versus TRANSP normalised toroidal flux radius X. (*b*) Fast ion density mapped on (R, Z) cross-section of the plasma. Magnetic flux surfaces are show in yellow, while the positions where the FI DF is calculated is noted by blue points. The reference case in table 1, is shown on the left; case #5 in table 1, which is without RF power, is shown on the right.

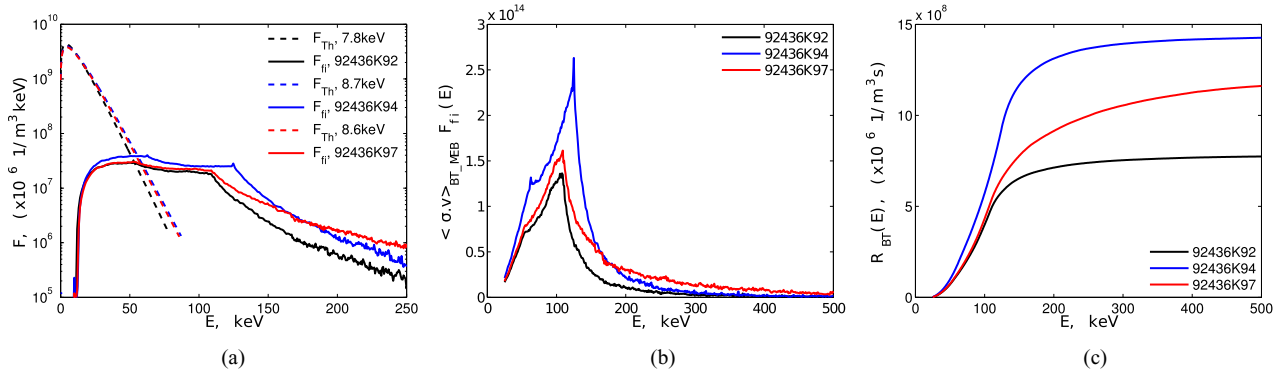

Figure 11. Baseline pulse #92436, 9.18 s, FI DF, $F_{\rm fi}$ (solid lines), and thermal Maxwellian distribution function, $F_{\rm Th}$ (dashed lines), in (*a*), the product $\langle\sigma \cdot v\rangle_{\rm BT\_MEB} F_{\rm fi}\,(E)$ in (*b*) and BT cumulative reaction rate $R_{\rm BT}(E)$ in (*c*) near magnetic axis at $R = 3$ m, $Z = 0.23$ m (position is also indicated by red dot in figure 10(*b*) for 92436K92 case). Reference case is in black, 4 MW higher NBI power is in blue and 4 MW higher RF power is shown by red lines.

power by 4 MW results in pedestal pressure changes by about 10%–15%.

5.2.1. Neutron yield changes with NBI and RF power. Modifications in parameters related to DD fusion performance with auxiliary heating power for #92436 are shown in table 1. Table 2 shows the result of power scan for #92395. In these power scans it was assumed that RF parameters and coupling are unchanged for RF power scans while NBI power changes via change in injected beam energy as for the reference cases with real power of about 27 MW NBI voltage was between 98 kV and 111 keV with average value of 106 kV. For $P_{\rm NB} = 23$ MW cases the injected beams were assumed to be at 95 kV, while for the high power cases of 31 MW beams voltage of 125 kV was used.

Reference cases correspond to the actual plasma pulses, #92436 and #92395, as modelled predictively by JETTO and interpretatively by TRANSP with results shown in figures 6–8. NBI and RF power variations in cases #1 to #6 are shown in columns 2 and 3 followed by fast ions, main ions and electron densities and temperatures, BT and thermal averaged reactivities and reaction rates. They are all volume averaged inside plasma volume $0 < X < 0.4$, where fusion reactions predominantly happen, see figure 4(*b*). Changes in BT and

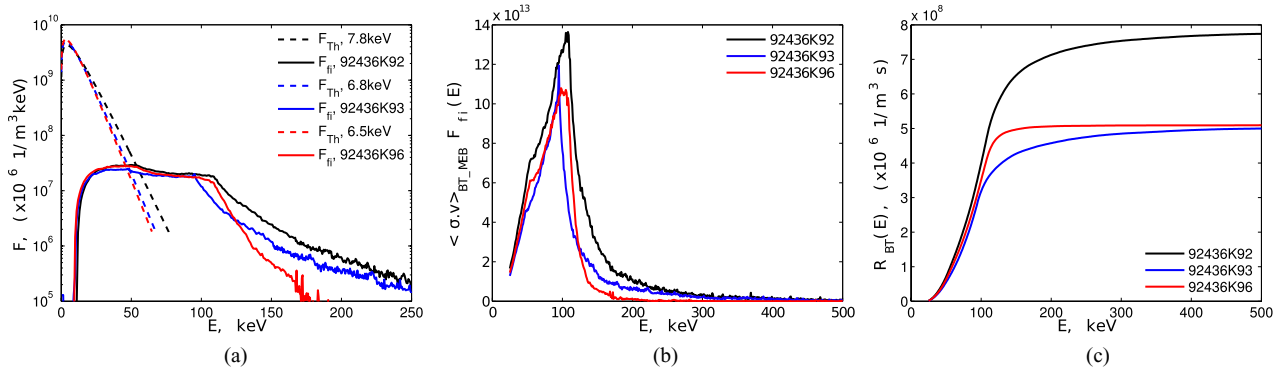

Figure 12. Same as figure 11 but for the case of lowering the NBI (blue) and RF (red) power by 4 MW.

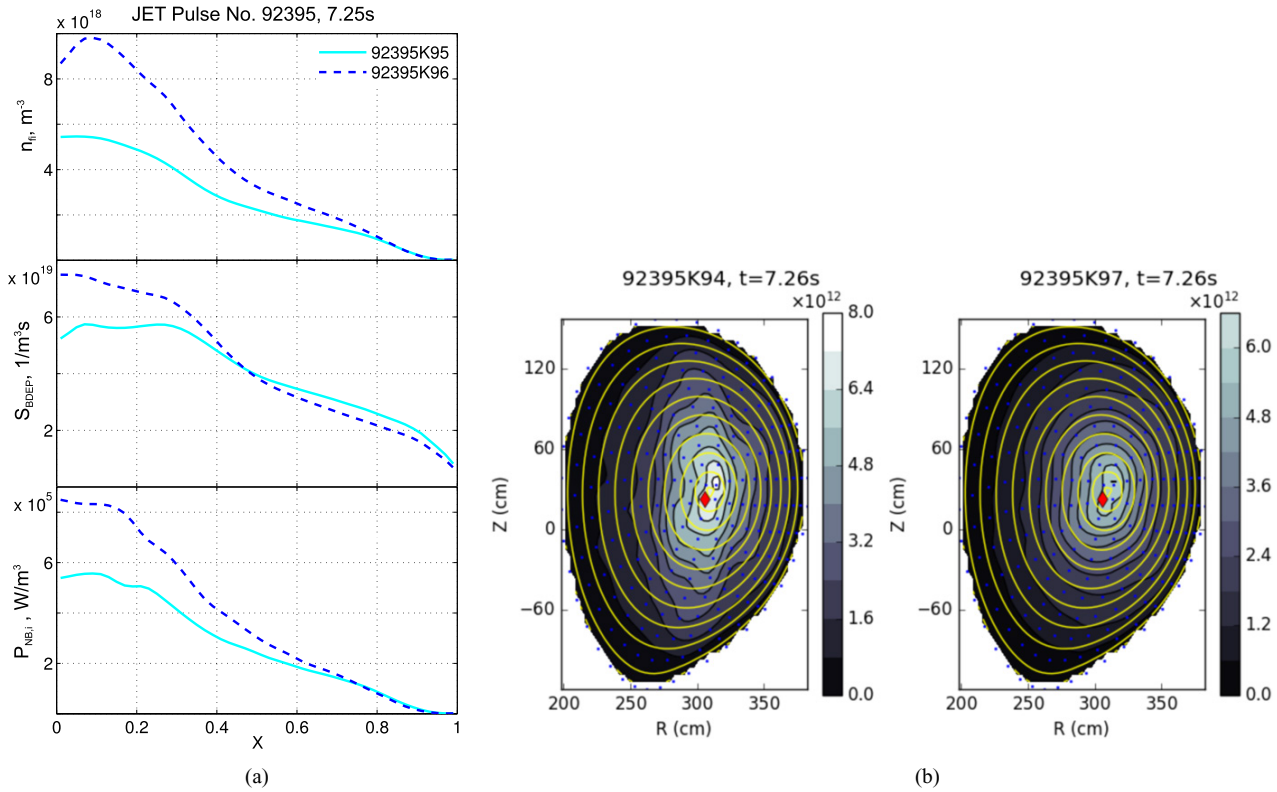

Figure 13. (*a*) Hybrid pulse #92395, simulations for $P_{NB} = 22.8$ MW, case #1 in table 2 (cyan solid lines), and $P_{NB} = 30.8$ MW, case #2 in table 2 (blue dashed lines), comparison of fast beam ion densities n_{fi} (top), beam deposition S_{BDEP} (middle) and NBI ion heating $P_{NB,i}$ (bottom). (*b*) Fast beam ion density mapped on (R, Z) cross-section of the plasma for the reference case in table 2 (left) and without RF power, case #5 in table 2 (right).

thermal reactivities and rates are taken from TRANSP at given time slice. TRANSP does not provide thermal reactivity, $\langle\sigma \cdot v\rangle_{Th}$, so an assessment of it is derived by dividing the reaction rate $\langle R_{Th}\rangle$ to $2\langle n_D\rangle^2$. BT, thermal and total number of neutrons are time averaged in the time interval indicated in the table. The top four rows of the tables give the results for NBI and RF power variation by 4 MW, while bottom two rows provide results from the $P_{RF} = 0$ cases discussed above.

Both NBI and RF powers affect insignificantly, less than 6%, n_D and n_e in all simulations presented in tables 1 and 2. The only exception is the case with $P_{RF} = 0$ (case #5) for the hybrid pulse #92395 in table 2, where n_D increases by about 7% if RF power is turned off. Having relatively small variations of n_D and n_e with power is a consequence of setting n_e at the TOB unchanged and only scaling T_e and T_i when varying pedestal pressure with input power. Normally, the plasma density is feedback controlled in experiments, so this assumption is meant to replicate the way in which an experiment will be conducted. Avoiding large variations of n_D has another advantage in our analysis as it eliminates the well-known dependences of the reaction rates on this parameter, i.e. linear for BT and square for thermal rates, thus focussing on dependencies related to T_e, T_i, n_{fi} and FI DF.

Considering the impact of NBI power on fusion performance for both scenarios, rows #1 and #2 in tables 1 and 2, one concludes that 4 MW of NBI power will cause large changes in $\langle n_{fi}\rangle$, 20%–37%, and averaged BT reactivity $\langle\langle\sigma \cdot v\rangle_{BT}\rangle$ changes by 17%–26%. Consequently, BT reaction rates

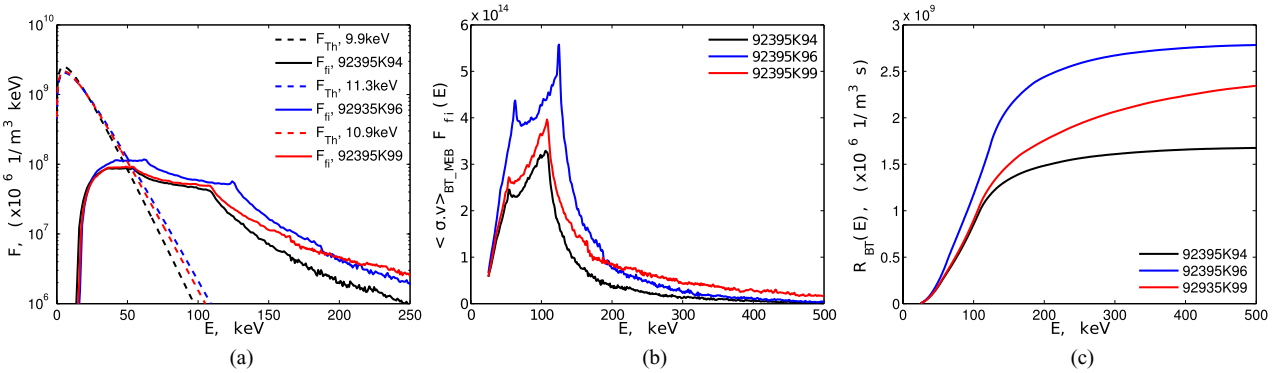

Figure 14. Hybrid pulse #92395, FI DF $F_{\rm fi}$ (solid lines) and thermal Mawellian DF $F_{\rm Th}$ (dashed lines) in (*a*), the product $\langle\sigma\cdot v\rangle_{\rm BT\_MEB}\,F_{\rm fi}$ (*b*) and BT cumulative reaction rate $R_{\rm BT}(E)$ in (*c*) near the magnetic axis, $R = 3$ m, $Z = 0.23$ m (position is also indicated by red dot in figure 13(*b*) for 92395K94 case). Reference case is in black, 4 MW higher NBI power is in blue and 4 MW higher RF power shown by red lines.

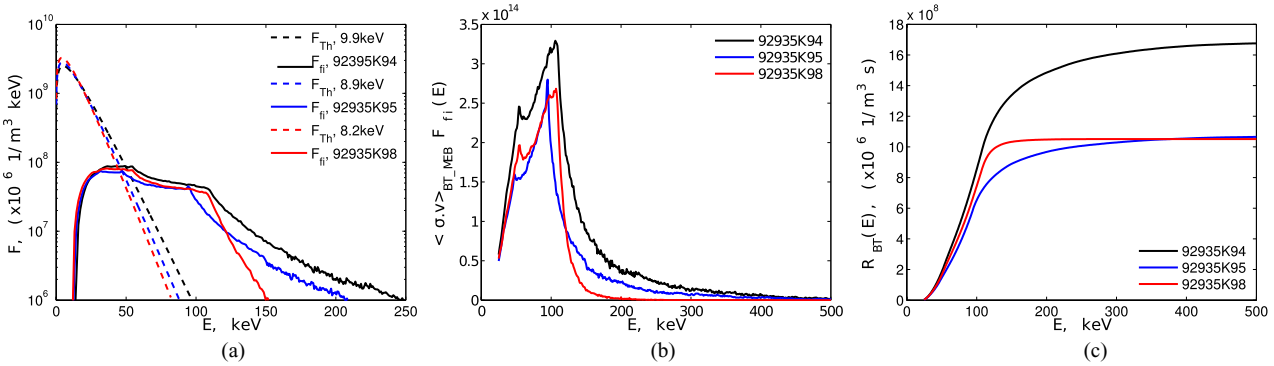

Figure 15. Same as the figure 14 but for the case of lowering the NBI (blue) and RF (red) power by 4 MW.

$\langle R_{\rm BT}\rangle$ are significantly affected by NBI power, 34%–74%. In addition, the thermal rate $\langle R_{\rm Th}\rangle$ also changes by about 24%–34% due to the impact of NBI on $T_{\rm i}$.

RF power impact is shown in rows #3, #4 in tables 1 and 2, and it affects mainly $T_{\rm e}$, $T_{\rm i}$ and averaged BT reactivity $\langle\langle\sigma\cdot v\rangle_{\rm BT}\rangle$ by 20%–27% and reaction rates $\langle R_{\rm BT}\rangle$ by 29%–39%. The latter is accompanied by changes in thermal reactivity $\langle\langle\sigma\cdot v\rangle_{\rm Th}\rangle$ by 24%–38% and rates $\langle R_{\rm Th}\rangle$ by 12%–36%. RF power will change $n_{\rm fi}$ considerably but to a lower extent compared to NBI power. The case with zero RF power, case #5, indicates the total effect of RF power. It shows that increase in neutrons with switching-on the RF power is due to combination of factors: $n_{\rm fi}$, $\langle\sigma\cdot v\rangle_{\rm BT}$, $T_{\rm e}$ and $T_{\rm i}$, the latter also directly affecting $\langle\sigma\cdot v\rangle_{\rm Th}$. All these contributions have comparable influences on neutron rate.

From tables 1 and 2 rows #1 to #4 one concludes that 4 MW of extra NBI power will produce an additional 50% neutrons. Increasing the RF power by the same amount will only deliver about 25% more neutrons. The main contributor to this enhancement is the BT rates which are more sensitive to changes in the NBI power. Although BT reactivity increases with fast ion energy, figure 5(*a*), it seems that in the investigated cases the RF power cannot generate enough fast particles to show a significant enhancement. In the conditions of the experiments shown here NBI power changes to the plateau of the FI DF seem to be more beneficial regarding the neutron rates. Changes in thermal rates reflect the changes in $T_{\rm i}$ with $P_{\rm NB}$ and $P_{\rm RF}$.

Comparing baseline to hybrid cases, one can conclude that $n_{\rm fi}$ changes with varying the heating power in a similar way for both scenarios. The same conclusion can be drawn for $T_{\rm e}$ and $T_{\rm i}$. Although $T_{\rm i}$ changes are similar the thermal reaction rate changes are different. For instance, from case #1 it follows that by dropping the NBI power by 4 MW, $T_{\rm i}$ will go down by 14% in baseline (table 1) and 11% (table 2) for hybrid pulse; however, $\langle\langle\sigma\cdot v\rangle_{\rm Th}\rangle$ is reduced by 33% and 25%, respectively. This could be due a number of factors, i.e. profile effects, different refence $T_{\rm i}$ and possibly stronger than square (~2.5) dependence of $\langle\langle\sigma\cdot v\rangle_{\rm Th}\rangle$ on $T_{\rm i}$. Interestingly, BT reactivity $\langle\langle\sigma\cdot v\rangle_{\rm BT}\rangle$ changes with heating power is similar in baseline scenario as it changes by the same amount independently of whether NBI or RF power is changed. In hybrid scenario the RF power changes affect $\langle\langle\sigma\cdot v\rangle_{\rm BT}\rangle$ slightly more strongly than corresponding NBI power variations.

Row #6 shows the changes in reactivities and rates if RF power is removed, but $n_{\rm e}$, $T_{\rm e}$ and $T_{\rm i}$ profiles are kept as in the reference case, while row #5 accounts for changes in these parameters with RF power. The aim of this comparison is to assess to what extent changes in kinetic profiles affect the thermal fusion performance and to differentiate them from synergistic effects due to changes in FI DF. From the numbers in rows #5 and #6 in tables 1 and 2 it can be concluded that

the RF synergistic effects of RF power on neutron yields are moderate for the investigated pulses. Fast ion density changes by only 5%, if RF power is removed but n_e, T_e and T_i profiles kept unchanged, row #6, while reactivity goes down by about 11%–13% and reaction rates by 15%–19%. Total neutron count drops by 5%–10% due to changes in BT neutrons of 9%–14%. In contrast to this, if changes in plasma parameters due to RF are taken into account, row #5, there is significant drop in both thermal and BT reactivities and reaction rates as shown in tables 1 and 2. The total neutron count in this case will drop by about 35%–41%. Clearly for the two pulses investigated here, the secondary effect accompanying application of RF power plays an important role in BT fusion performance.

5.2.2. Fast ion densities and distribution function. The causes of the observed dependencies are further analysed by examining n_{fi}, beam depositions and heating profiles and FI DF in the plasma core.

Varying the NBI power by 4 MW, cases #1 and #2 in table 1, results in significant changes in n_{fi}, beam deposition and NBI ion heating, figure 10(*a*). The beam deposition profile changes from off-axis for lower P_{NB} and beam energy to a flat profile for $P_{NB} = 31.6$ MW.

Comparing the reference case with the 'without RF' power case #5, one sees similar NBI electron and ion heating as well as same beam deposition; however, fast ion density is higher in the core with RF power. The plasma (R, Z) cross-sections shown in figure 10(*b*) confirm this conclusion and show distribution of fast ions along the IC resonance when RF power is applied. Fast ion density becomes highly inhomogeneous when RF power is applied. This observation is qualitatively consistent with the gamma-ray imaging diagnostic on JET [59]. The increase in n_{fi} in the core for the reference case compared to zero RF power case is due to RF power pulling high energetic tail and fast particles become less collisional. This conclusion is also confirmed by examining case #6 in table 1 compared to the reference case. Increase in n_{fi} with RF power in this case is purely due to generating more high energy particles which have larger slowing down time thus increasing n_{fi}.

Changes in FI DF in the core for baseline scenario #92436 after increasing or decreasing NBI and RF power by 4 MW are shown in figures 11 and 12. Reference case is in black, cases where changes to the NBI power is made are in blue, while RF power scans are in red. In addition, the product $\langle\sigma \cdot v\rangle_{BT\_MEB} F_{fi}$ and BT cumulative reaction rate $R_{BT}(E)$ are shown in order to illustrate which part of affected FI DF impacts most on the reaction rates.

Following the red lines in figure 12 it is clear that by decreasing the RF power by 4 MW (case #3 in table 1) FI DF tail will be largely reduced, red lines in figure 12(*a*). This will lead to FI DF tail practically having no contribution to the BT reactivity as seen in figure 12(*b*) with red line nearly zero, while the cumulative integral in figure 12(*c*) is constant for energies $E > 110$ keV. It is estimated that about 83% of the averaged reactivity is provided by fast ions with energies up to 110 keV and only 17% by fast ions with energies above 110 keV. On the other hand, increasing the RF power (case #4 in table 1) will create a larger tail as seen when comparing the black and red lines in figure 11(*a*). This will ultimately change $R_{BT}(E)$ for energies above the beam energy, E_b, as shown in figure 11(*b*). One should note that the latter is now significantly larger and above zero for $E > 110$ keV. It is clear from figure 11(*c*) following the red line that contributions from particles with energies in the range 110–500 keV to the BT reactivity is significant, 56%, for RF power increase by 4 MW. The total increase of R_{BT} due to RF power in figure 11(*c*) is about 48% which is slightly higher than the flux surface averaged value of 39% in table 1 row #4. The latter shows that the BT rates enhancement with RF power is localised in the core and to some extent along the IC resonance line, figure 10(*b*).

The impact of the NBI power on the FI DF and BT reaction rate differs qualitatively from the aforementioned case. Comparing the black and the blue lines in the case where NBI power was increased by 4 MW, figure 11(*a*), or reduced by the same amount, figure 12(*a*), one sees that the NBI power mainly affects the plateau region of the FI DF, while the gradient of the tail is practically unchanged. The latter is determined by the fast ion slowing down, so the FI DF tail gradient for $E > E_b$ depends on T_e and T_i. The plateau changes in two ways: (i) the high energy end is pushed towards higher energies with beam energy and power and (ii) the plateau is lifted up with NBI power. One can conclude in this case that the changes in the BT rate is mainly due to changes in the FI DF in the beam energy range, up to 95 keV for case #1 (table 1) with $P_{NB} = 23.4$ MW, 110 keV for reference case with $P_{NB} = 27.5$ MW and 125 keV for case #2 with $P_{NB} = 31.6$ MW. In all these cases fast ions in the plateau of the distribution function contribute nearly two thirds (67% for case #2 to 61% for case #1) to the BT reactivity.

As with baseline, in hybrid pulse #92395 higher NBI power by 4 MW, case #2 in table 2, results in higher electron and ion heating; fast ion density and beam deposition are higher in the core compared to the lower power case with P_{NB} reduced by 4 MW, figure 13(*a*).

Similar NBI electron and ion heating as well as beam deposition were observed when comparing the reference case with no RF power case. Fast ion density is higher in the core with RF power. (R, Z) plasma cross-sections in figure 13(*b*) confirm this conclusion and show enhanced distribution of fast ions along IC resonance when RF power is applied.

Case #5 with zero RF power shows that an increase in neutrons commensurate with switching on the RF power is due to a combination of factors: n_{fi}, $\langle\sigma \cdot v\rangle_{BT}$, T_e and T_i affecting $\langle\sigma \cdot v\rangle_{Th}$ all having comparable contributions.

Changes in FI DF in the core for hybrid pulse #92395 after changing the auxiliary heating power by 4 MW are shown in figures 14 and 15. The product $\langle\sigma \cdot v\rangle_{BT\_MEB} F_{fi}$ and BT cumulative reaction rate $R_{BT}(E)$ are shown as well.

Similar to the baseline case, RF power (red lines in figures 14(*a*) and 15(*a*)) affects to the largest extent the tail of the FI DF. By increasing the RF power from 1 MW to 5 MW and then to 9 MW the contribution of energetic particles with $E > 120$ keV to the BT reactivity becomes dominant as seen from the red curves figures 14(*b*) and 15(*b*). At the highest RF power (case #4 of table 2 and red line in figure 14 c))

energetic particles with $E > 110$ keV provide more than half, 54%, of BT neutrons, while for the lowest RF power only about 16% of the integral of $\langle\sigma \cdot v\rangle_{BT} F_{fi}$ comes from particles in the tail, case #3 of table 2 and red line in figure 15(*c*).

NBI power impacts mainly on the FI DF plateau, the higher energy end of which extends further with power as beam energy increases. The tail in the distribution function also changes but its slope remains relatively unchanged with P_{NB}, blue and black lines in figures 14(*a*) and 15(*a*). The contribution of the plateau to the BT reactivity slightly changes with NBI power, about 62% for the highest P_{NB} (case #2 in table 2 with 30.8 MW and blue line in figure 14(*c*)) to about 56% for the lowest NBI power (case #1 in table 2 and blue line in figure 15(*c*)).

It is obvious from figures 11 and 14 following the red curves that in the conditions of the best performing baseline and hybrid pulses RF power can generate an energetic tail in the FI DF to provide up to about half of the BT neutrons. In some cases, however, BT fusion performance enhancement due to synergistic effects can be much higher. For instance, in the three ion heating experiments performed recently at JET [60] very high energy tail in FI DF in this case is found to be responsible for more than 90% of generated DD neutrons.

6. Conclusions

Changes in auxiliary heating power, NBI and RF, by 4 MW against background of about 33 MW will affect DD fusion performance and neutron rates significantly in both scenarios studied here: baseline and hybrid. This will come through changes in bulk plasma parameters, T_e and T_i, as well as in fast ion density and distribution function. Changes in ion temperature, T_i, will naturally affect thermal neutrons, while in addition changes to the FI DF will have an impact on BT neutrons. Thermal reaction rates, R_{Th}, change within 12% to 60%. Tables 1 and 2 show significant changes of averaged BT reactivities, $\langle\sigma \cdot v\rangle_{BT}$, and reaction rates, R_{BT}, more that about 20% in all cases, resulting in changes in BT neutrons, N_{BT}, between 30% and 60%. The total neutron yields, N_{TOT}, vary within 25% to 52%.

The impact of the RF and NBI power on the BT reactivities $\langle\langle\sigma \cdot v\rangle_{BT}\rangle$ was found to be of similar magnitude. From these observations one can conclude that in NBI and RF plasma it is equally efficient for the DD BT reactions to act on the FI DF plateau by further increasing the NBI power or to pull a high energy tail in the FI DF by applying higher RF power. Despite similarities in $\langle\langle\sigma \cdot v\rangle_{BT}\rangle$ variations with NBI and RF power, it has been observed that NBI power has greater impact than RF regarding $\langle R_{BT}\rangle$ and N_{BT} changes. This is attributed to the larger increase in n_{fi} with P_{NB} than with RF.

Investigating the pure impact of RF power by using the kinetic profiles from reference pulses but turning off the RF heating shows a moderate impact of the RF synergistic effects on the BT fusion performance, normally a drop by about 10% in neutron rate is observed if RF power is removed. The secondary effect accompanying application of RF power, i.e. changes in T_e and T_i, play an important role in both thermal and BT fusion performances. Examining the cumulative rates show that the RF tail in the modelled FI DF in the investigated high-performance pulses is not sufficiently large to provide significant enhancement in the high energy range on the fast ions.

Based on the simulations, one can conclude that both scenarios, baseline and hybrid, will equally benefit from synergistic effects. Both scenarios will benefit from adding 4 MW of extra power to the reference pulses with NBI power change having larger effect on neutron yield than RF. Dropping the RF power however will have a massive negative impact regarding fusion performance of both scenarios. An interesting observation is that similar changes in T_i will inflict larger impact on thermal yield for baseline compared to hybrid. Also comparing the two scenarios it seems hybrid will compensate the smaller increase in thermal yield by larger increase in BT neutrons with power.

Regarding planning future experiments with the goal of achieving maximum DD fusion performance, the simulations point out that for the baseline scenario an effort to increase the NBI power will be more beneficial, while RF power should not be dropped below 5–6 MW. Similar conclusions can be drawn for the hybrid pulses. Providing that changes in BT reactivities with NBI and RF power are of the same order, clearly the conclusion that NBI will have more beneficial impact on BT reaction rate is based on the fact that n_{fi} increases more with P_{NB} than with P_{RF}.

The scope of the study can be further extended in analysing the RF parameter space, e.g. minority scheme and concentrations, antenna phasing, etc. A challenging part of these studies will be to analyse DT mixture plasma. It will require better understanding of the isotope effect on the transport, confinement and pedestal physics scaling. This investigation can eventually provide the necessary predictive capabilities for the forthcoming DT campaign at JET.

Acknowledgment

This work has been carried out within the framework of the EUROfusion Consortium and has received funding from the Euratom research and training programme 2014–2018 under grant agreement No. 633053. The views and opinions expressed herein do not necessarily reflect those of the European Commission.

ORCID iDs

J. Eriksson https://orcid.org/0000-0002-0892-3358
L. Garzotti https://orcid.org/0000-0002-3796-9814

References

[1] Noterdaeme J.-M. *et al* 1998 *Fusion Energy 1998 (Proc. 17th Int. Conf. Yokohama, 1998)* (Vienna: IAEA) CD-ROM file and http://www.iaea.org/programmes/ripc/physics/start.htm
[2] Messiaen A.M. *et al* 1993 *Plasma Phys. Control. Fusion* **35** A15–34

[3] Mantsinen M. *et al* 2004 *Nucl. Fusion* **44** 33
[4] van Eester D. *et al* 2009 *Plasma Phys. Control. Fusion* **51** 044007
[5] Lerche E. *et al* 2009 *Plasma Phys. Control. Fusion* **51** 044006
[6] Schneider M. *et al* 2016 *Nucl. Fusion* **56** 112022
[7] Henriksson H. *et al* 2006 *Nucl. Fusion* **46** 244
[8] Kimura H. *et al* 1991 *Nucl. Fusion* **31** 83
[9] Bilato R. *et al* 2011 *Nucl. Fusion* **51** 103034
[10] Gallart D. *et al* 2017 *22nd Topical Conf. on Radio-Frequency Power in Plasmas (Aix-en-Provence, France, 30 May–2 June 2017)* (https://doi.org/10.1051/epjconf/201715703015)
[11] Mantsinen M. *et al* 2017 *Eur. J. Phys.* **157** 03032
[12] Gallart D. *et al* 2017 *Eur. J. Phys.* **157** 03015
[13] Gallart D. *et al* 2018 *Nucl. Fusion* **58** 106037
[14] Jacquinot J. and JET Team 1998 *Nucl. Fusion* **38** 1263
[15] Cottrell G.A. *et al* 1989 *Plasma Phys. Control. Fusion* **31** 1727
[16] Eriksson L.-G. *et al* 1999 *Nucl. Fusion* **39** 337
[17] Mantsinen M. *et al* 2001 *Nucl. Fusion* **41** 1815
[18] Cottrell G.A., Rimini F.G. and JET Team 1999 *Nucl. Fusion* **39** 2025
[19] Start D.F.H. *et al* 1999 *Nucl. Fusion* **39** 321
[20] Start D.F.H. *et al* 1998 *Phys. Rev. Lett.* **80** 4681
[21] Start D.F.H. and JET Team 1998 *Plasma Phys. Control. Fusion* **40** A87
[22] Meade D.M. and the TFTR team 1994 *J. Fusion Energy* **13** 145
[23] Budny R.V. *et al* 1995 *Nucl. Fusion* **35** 1497
[24] Joffrin E. and JET Contributors 2018 Preprint: *2018 IAEA Fusion Energy Conf. (Gandhinagar, India, 22–27 October, 2018)* OV/1-3
[25] Fasoli A. *et al* 2007 Progress in the ITER Physics Basis: Chapter 5: Physics of energetic ions *Nucl. Fusion* **47** S264
[26] ITER Physics Expert Group on Energetic Particles Heating and Current Drive, ITER Physics Basis Editors: Chapter 6: Plasma auxiliary heating and current drive 1999 *Nucl. Fusion* **39** 2495
[27] Garcia J. *et al* 2018 Preprint: *2018 IAEA Fusion Energy Conf. (Gandhinagar, India, 22–27 October, 2018)* TH/3-1
[28] Doyle E.J. *et al* 2007 Progress in the ITER Physics Basis: Chapter 2: Plasma confinement and transport *Nucl. Fusion* **47** S18
[29] Garzotti L. *et al* 2018 Preprint: *2018 IAEA Fusion Energy Conf. (Gandhinagar, India, 22–27 October, 2018)* EX/3-6
[30] Romanelli M. *et al* 2014 *Plasma Fusion Res.* **9** 3403023
[31] Erba M. *et al* 1997 *Plasma Phys. Control. Fusion* **39** 261
[32] Eriksson L.-G. *et al* 1993 *Nucl. Fusion* **33** 1037
[33] Stubberfield P. and Watkins M 1987 *JET-DPA* **06** 87
[34] Challis C. 1989 *Nucl. Fusion* **29** 563
[35] Mantsinen M. *et al* 1999 *Plasma Phys. Control. Fusion* **41** 843
[36] Hawryluk R.J. *et al* 1980 An empirical approach to tokamak transport *Physics of Plasmas Close to Thermonuclear Conditions* vol 1, ed B. Coppi *et al* (Brussels: CEC) pp 19–46
[37] Budny R.V. *et al* 1992 *Nucl. Fusion* **32** 429
[38] http://w3.pppl.gov/transp
[39] Grierson B.A. *et al* 2018 *Fusion Sci. Technol.* (https://doi.org/10.1080/15361055.2017.1398585)
[40] Pankin A. *et al* 2004 The tokamak Monte Carlo fast ion module NUBEAM in the national transport code collaboration library *Comput. Phys. Commun.* **159** 157–84
[41] Brambilla M. 1999 *Plasma Phys. Control. Fusion* **41** 1
[42] Hammett G.W. 1986 Fast ion studies of ion cyclotron heating in the PLT tokamak *PhD Thesis* Princeton
[43] Kwon J.-M., McCune D. and Chang C.S. 2007 Enhancement of NUBEAM for the simulation of fast ion and RF-wave interaction based on the quasi-linear theory, Bulletin of the American Physical Society *49th Meeting of the Division of Plasma Physics (Orlando, FL)* (http://meetings.aps.org/link/BAPS.2007.DPP.UP8.83)
[44] Kwon J.-M., Chang C.S., Ku S., McCune D. and Phillips C.K. 2006 Development of XGC-RF for global guiding-center particle simulation of minority ICRH heated Plasmas in a General Tokamak Geometry, Bulletin of the American Physical Society *48th Meeting of the Division of Plasma Physics (Philadelphia, PA)* (http://meetings.aps.org/link/BAPS.2006.DPP.VP1.115)
[45] Budny R. and Gorelenkova M. 2015 *57th Annual Meeting of the APS Division of Plasma Physics (Savannah, GA, 16–20 November 2015)* vol 60 p GP12.00127
[46] Gowers C. *et al* 1995 *Rev. Sci. Instrum.* **66** 471
[47] de la Luna E. *et al* 2001 *Rev. Sci. Instrum.* **74** 1414
[48] Kim H.-T. *et al* 2018 *Nucl. Fusion* **58** 036020
[49] Czarnecka A. *et al* 2018 *Plasma Phys. Control. Fusion* submitted
[50] Gatu Johnson M. *et al* 2008 *Nucl. Intrum. Methods* A **591** 417
[51] Hellesen C. *et al* 2010 *Plasma Phys. Control. Fusion* **52** 085013
[52] Eriksson J. *et al* 2016 *Comput. Phys. Commum.* **116** 40–6
[53] Mikkelsen M. *et al* 1989 *Nucl. Fusion* **29** 1113
[54] Casson F.J. *et al* 2018 Preprint: *2018 IAEA Fusion Energy Conf. (Gandhinagar, India, 22–27 October, 2018)* TH/3-2
[55] Bourdelle C. *et al* 2016 *Plasma Phys. Control. Fusion* **58** 014036
[56] Goniche M. *et al* 2017 *Plasma Phys. Control. Fusion* **59** 055001
[57] Cordey J.G. *et al* 2003 *Nucl. Fusion* **43** 670
[58] Frassinetti L. *et al* 2018 *45th EPS Conf. on Plasma Physics (Prague, Czech Republic, 2–6 July 2018)* p P4.1027
[59] Kiptily V.G. *et al* 2005 *Nucl. Fusion* **45** L21
[60] Kazakov Ye. *et al* 2015 *AIP Conf. Proc.* **1689** 030008
[61] Litaudon X. *et al* 2017 *Nucl. Fusion* **57** 102001